Published in final edited form as:

Curr Biol. 2020 June 22; 30(12): 2275–2288.e5. doi:10.1016/j.cub.2020.04.038.

A circuit encoding absolute cold temperature in *Drosophila*

Michael H. Alpert[†], **Dominic D. Frank**[†], **Evan Kaspi**, **Matthieu Flourakis**, **Emanuela E. Zaharieva**, **Ravi Allada**, **Alessia Para**, **Marco Gallio**[*]

Department of Neurobiology, Northwestern University, Evanston, Illinois, 60208, USA,

SUMMARY:

Animals react to environmental changes over time scales ranging from seconds to days and weeks. An important question is how sensory stimuli are parsed into neural signals operating over such diverse temporal scales. Here, we uncover a specialized circuit, from sensory neurons to higher brain centers, that processes information about long-lasting, absolute cold temperature in *Drosophila*. We identify second-order thermosensory projection neurons (TPN-IIs) exhibiting sustained firing that scales with absolute temperature. Strikingly, this activity only appears below the species-specific, preferred temperature for *D. melanogaster* (~25°C). We trace the inputs and outputs of TPN-IIs, and find that they are embedded in a cold "thermometer" circuit that provides powerful and persistent inhibition to brain centers involved in regulating sleep and activity. Our results demonstrate that the fly nervous system selectively encodes and relays absolute temperature information, and illustrate a sensory mechanism that allows animals to adapt behavior specifically to cold conditions on the timescale of hours to days.

Graphical Abstract

[*]Lead contact: marco.gallio@northwestern.edu.

[†]Equal contributors

AUTHOR CONTRIBUTIONS

M.G., M.A. and D.F. designed the study, analyzed the data, and wrote the paper with critical input from all authors; M.A. performed all recordings with initial assistance from M.F, and Ca^{2+} imaging for F1. D.F. performed circuit mapping, Ca^{2+} imaging (F3) and anatomy. E.K. performed and analyzed sleep and activity recordings with assistance from M.A. E.Z. performed immunohistochemistry. A.P. assisted with recombinant and transgenic reagents. R.A provided critical expertise.

DECLARATION OF INTERESTS

The authors declare no competing interests.

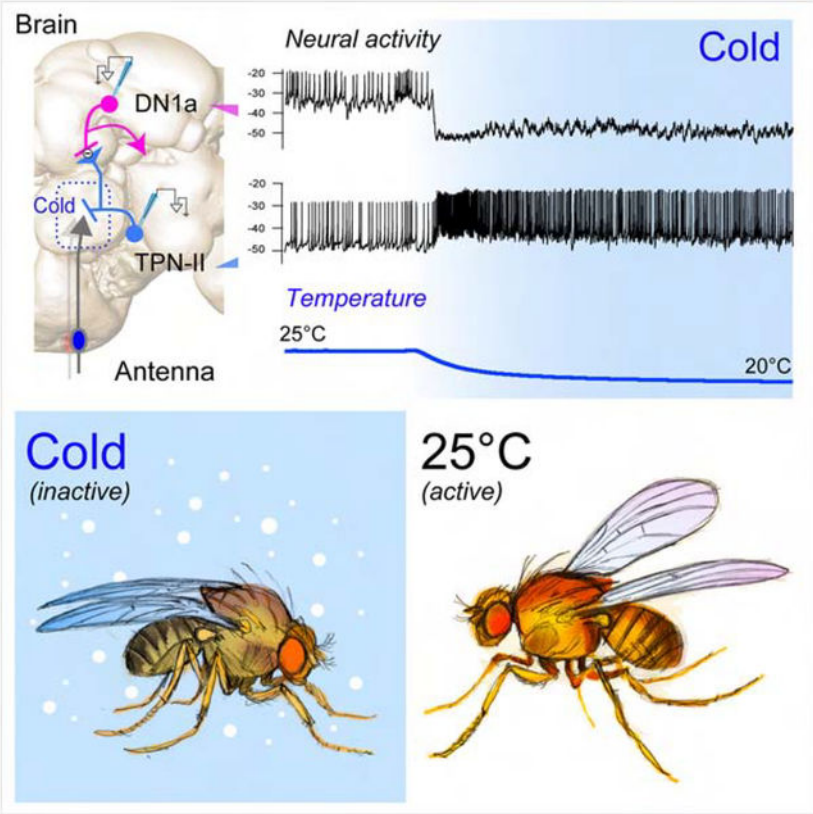

eTOC Blurb

Alpert *et al.* uncover a specialized circuit, from sensory neurons to higher brain centers, that processes information about absolute cold temperature in *Drosophila*. This circuit directly connects thermosensory neurons of the antenna with circadian and sleep centers in the brain, adapting sleep and activity specifically to cold conditions

INTRODUCTION

Changes in temperature influence animal behavior on both short (seconds to minutes) and long (hours to days and weeks) timescales. Rapid changes in the external temperature are transformed by the nervous system into the percepts of heating and cooling and used to quickly predict and avoid potentially dangerous thermal extremes. Meanwhile, sustained thermal conditions below or above the optimal range (perceived as cold or hot, respectively) trigger specific long-term behavioral and autonomic responses including shivering or sweating, changes in sleep/wake patterns, and seasonal adaptations such as hibernation or aestivation. Little is known on how these responses, happening on vastly different temporal scales, are orchestrated in the brain starting from the activity of peripheral thermosensory neurons.

The debate on how absolute temperature and temperature change are encoded in the nervous system is an old one, and one that is central to our understanding of how sensory stimuli are processed on different timescales. Having observed robust adaptation as a result of

prolonged exposure to cold temperature in humans, in the 1800s Weber argued that only temperature changes and not absolute temperature stimulate thermosensory neurons [1]. In 1950, Hensel and Zotterman rebuked this notion, presenting data from cold receptors of the skin that showed a burst of firing in response to cooling, but also persistent activity in response to stable cold [2]. This led to the idea that temperature change and absolute temperature information could be extracted from the complex activity of sensory neurons [3], but this has been difficult to prove experimentally in the absence of specific assays and reagents that would allow one to dis-entangle transient from persistent signals.

Recent advances in microscopy and the availability of activity indicators have made it possible to systematically characterize the responses to temperature simultaneously in large numbers of neurons of the mouse trigeminal ganglion (innervating the oral cavity [4]) and dorsal horn of the spinal cord (receiving input from neurons innervating the skin [5]). The results revealed an unanticipated complexity - with multiple functionally distinct classes of responses characterized by different adaptation properties and thresholds of activation. However, it is fair to say that, even after more than two hundred years of work in this area, we still do not understand how information about temperature change and absolute temperature may be differentially extracted from the activity of sensory neurons at the periphery and relayed to the brain to trigger the appropriate responses.

Drosophila flies are small poikilothermic animals and are characterized by robust temperature evoked-behavior and a numerically simpler nervous system. On account of these advantages, work in the fruit fly is providing fundamental insights into the basic principles of temperature sensing and processing in the brain.

In flies, rapid temperature changes are detected by thermosensory neurons residing in the last antennal segment, the arista [6]. Each arista contains three thermosensory sensilla, each housing one hot- and one cold-activated cell. Much like their mammalian counterparts, antennal TRNs respond to the preferred temperature stimulus (cooling for cold-activated TRNs etc.) with activity that generally scales with stimulus intensity. Non-preferred stimuli instead cause a decrease in intracellular calcium [6] and firing rates [7].

From their origin at the periphery, the axons of hot- and cold-activated TRNs of the arista converge onto a brain region called the posterior antennal lobe (PAL), where they form adjacent “hot” and “cold” glomeruli defining a simple sensory map for the central representation of external temperature [6]. Next in line, second order thermosensory projection neurons (TPNs) collect information from the PAL glomeruli and target higher brain centers involved in the processing of both innate and learned behavior [8, 9].

Interestingly, TPN cell types are characterized by different response dynamics to temperature stimuli: “fast-adapting” cells respond rapidly but transiently to the onset of a temperature change, while “slow-/ non-adapting” TPNs are characterized by persistent activity [8, 9]. Differences in TPN adaptation dynamics are potentially very significant, as “fast-adapting” TPNs may relay temperature change signals, while “slow-adapting” cells are well-positioned to relay information about absolute temperature.

How are temperature change and absolute temperature signals encoded in the activity of TPNs, relayed to higher-brain circuits, and used to inform behavior happening on timescales ranging from milliseconds to seconds, to days and weeks?

Here, focusing on cold responses, we set out to identify the source and significance of the persistent activity observed in “slow-adapting” TPNs. Our ultimate goal was to understand how the thermosensory system may process information about absolute temperature and how this information may be used to drive behavior happening on the appropriate timescales.

Our work leads to the identification of a circuit that functions as a conduit for information about absolute temperature in the cold range. This circuit displays persistent activity that scales with temperature, but only at absolute temperatures lower than the fly’s favorite ~25°C, and directly targets higher brain centers involved in the control of sleep and activity, adjusting fly behavior specifically to cold conditions.

RESULTS

A thermosensory PN displays persistent activity in response to extended cold steps

To systematically study the adaptation dynamics of TPNs, we focused on two cold-activated TPN cell types previously described as “fast-” and “slow-” adapting (TPN-I and II in Figure 1A, identified by expression of the drivers VT19428 and R60H12, respectively [8]). We designed a stimulation protocol that consists of a rapid temperature change (~2°C/second) followed by extended stable “cold” conditions (1–15 minutes), again followed by a rapid return to baseline. As before, we initially chose as the baseline the fly’s preferred temperature of 25°C, and stimulus parameters (rate of change and temperatures ranges) reasonably close to what a fly may encounter in the environment. We then used two-photon calcium imaging and recorded TPN responses to temperature stimulation, by targeting expression of the transgenic calcium indicator GCaMP to each cell type (i.e. under the control of selective drivers [8]).

Our results demonstrate that calcium levels in fast-adapting VT19428 TPNs quickly return to baseline after an initial cooling-induced spike (TPN-Is, Figure 1B). In contrast, R60H12 TPNs (TPN-IIs) respond to a cold temperature step with an initial calcium spike that accompanies the onset of cooling and that is followed by a rapid decrease to a plateau. The levels of intracellular Ca^{2+} do not return to baseline for as long as the temperature remains in the cold range (Figure 1C), supporting the notion that these cells may not adapt at all under conditions of persistent cold.

Calcium levels do not allow one to estimate the firing rate of a neuron in stable conditions. To obtain a more direct read-out of TPN-II’s action potential firing under conditions of persistent cold, we next developed a method to perform two-photon guided patch clamp electrophysiology, by targeting TPN-IIs using GFP expression as a guide (again under the control of the selective driver R60H12-Gal4 [8]).

Our patch clamp results confirmed and expanded what we had observed using calcium imaging. The firing rate of non-adapting TPN-IIs showed little or no evidence of adaptation; rather, TPN-IIs sustained a remarkably stable level of activity for the entire duration of the cold step. Only when the temperature started returning to baseline TPN-II's firing rate decreased, followed by a small inflection in membrane potential (Figure 1D,E; note that heating steps caused little response in TPN-IIs, Figure 1F,G). Protracted patch-clamp recordings further demonstrated that TPN-IIs display little or no adaptation even to extended cold stimuli (~25 minutes, Figure 1H–J).

TPN-II activity correlates with absolute temperature in the cold range

Our next goal was to determine if the persistent activity of non-adapting TPN-IIs at stable cold conditions indeed scales proportionally with (and may therefore contain information about) "absolute" temperature, rather than correlate with other stimulus statistics such as the magnitude of the initial cooling change (Δt).

To address this question, we designed temperature steps which either differed in the absolute temperature reached at stable conditions (different |t|, same Δt), or in the magnitude of the temperature change the preparation experiences on the way to the same stable conditions (different Δt, same |t|).

Our data show that the firing rate of non-adapting TPN-IIs at stable conditions (persistent activity) correlates with absolute temperature, rather than with stimulus history (Figure 2). Remarkably, while an initial action potential burst (dynamic activity) was invariably observed in response to cooling (Figure 2A–D), persistent activity (i.e. "plateau" firing rates above baseline firing) only appeared when the absolute temperature stabilized at temperatures lower than 25°C (Figure 2B,D,E), i.e. lower than the preferred temperature for *Drosophila melanogaster*. Even when challenged with prolonged stimuli involving multiple cooling steps, static activity only emerged below 25°C (Figure 2F), and only in this range firing rates correlated well with absolute temperature (Figure 2G,H).

These observations suggest that the non-adapting activity of TPN-IIs may indeed encode information about absolute temperature below the preferred range for *D. melanogaster*, i.e. in what can be described as "cold" temperature for the fly.

The PAL cold glomerulus is independently targeted by distinct populations of thermosensory neurons

Our results raise a number of important questions: where does this "absolute" cold temperature signal originate (at the sensory layer or within TPNs)? And what may be the behavioral significance of such a persistent "cold"-evoked activity in the fly brain? We set out to address each question in turn.

First, we re-evaluated the contribution of the sensory neurons of the antenna to TPN-II cold responses. Consistent with previous observations [8, 9], acute resection of the antennal nerve completely abolished TPN-II responses (Figure S1) suggesting that all cold-evoked activity originates in thermosensory neurons of the antenna (rather than within TPN-IIs).

We reasoned that any sensory input into TPN-IIs would have to come from neurons innervating the cold glomerulus of the PAL (harboring the post-synaptic terminals of TPN-IIs; Figure 3A,B), and screened a collection of Gal4 lines for drivers that would allow us to identify and selectively manipulate sensory input to this TPN cell type.

We discovered that at least 3 cell types independently target the cold glomerulus of the PAL: (*1*) the well-known TRNs of the arista ([6], labeled by a selective driver in Figure 3C,D); (*2*) a new population of sensory neurons which innervate chamber one of the sacculus, a structure previously shown to be involved in olfaction and humidity sensing ([10, 11], labeled by a selective driver in Figure 3E,F); and, (*3*) an unusual cell type that expresses the broad sensory co-receptor IR25a and that resides at the margin of the antennal nerve (note that the terminals of this cell type within the PAL are clearly visible after ablation of the antenna, i.e. as a result of degeneration of all other antennal afferents, Figure 3G,H). The location of this cell is similar to that of the previously described “Anterior Cell” neurons [12], and we therefore refer to it as the Anterior Cold Cell (ACc, Figure 3H inset–and see Figure S2 for further characterization of this unusual sensory neuron).

The observation that additional sensory cell types (besides the aristal TRNs [6]) converge onto the cold glomerulus of the PAL was unexpected: we have previously described cold-responding sensory neurons innervating sensilla located in chamber two of the sacculus, but these neurons are part of an “hygrosensory triad” (composed of a dry- a humid- and a cold-activated cell innervating the same sensillum) and project to a distinct region of the PAL (the “column” or VP1 glomerulus [10, 11]). The results of 2-color two-photon microscopy instead suggest extensive intermingling between TPN-II dendrites, the terminals of chamber one sacculus neurons, and those of arista TRNs within the cold glomerulus of the PAL (Figure 3I–O). Finally, we were surprised to find an additional “internal” temperature receptor within the head capsule (ACc, see above) which also selectively innervates the cold glomerulus. Our results confirm that each of these cell types independently innervating the “cold” glomerulus indeed selectively responds to cold temperature stimuli (see below).

Multiple pre-synaptic drives shape the activity of TPN-IIs

Our next goal was to determine if each of the sensory neurons innervating the cold glomerulus indeed provides direct synaptic drive to TPN-II. To test for connectivity, we employed activity-dependent, synaptic GFP Reconstitution Across Synaptic Partners (syb:GRASP) [13].

Our results suggest that each sensory cell population makes direct functional connections with TPN-II second-order neurons (Figure 3P–R). Using selective drivers, we could directly demonstrate synaptic GFP reconstitution between chamber one sacculus neurons and TPN-IIs (Figure 3P). We have been so far unable to identify a driver only active in ACc neurons; to test for ACc:TPN-II connectivity, we used R77C10-Gal4 -a driver active in both the arista cold-activated TRNs and ACc neurons. Robust GFP reconstitution using this line confirmed that one or both of these cell types indeed forms synapses with TPN-IIs (Figure 3Q, and see [8, 9] for arista TRNs:TPN-II connectivity). Moreover, significant syb:GRASP signal persisted even a week following antenna ablation (i.e. following degeneration of antennal

afferents, Figure 3R). This result suggests that AC cells are also independently connected to TPN-IIs.

Chamber I sacculus neurons selectively respond to absolute cold

Next, we asked which –if any- of these cold sensing cell types may contribute the "absolute" cold temperature signal recorded in TPN-IIs. To address this question, we designed a stimulation protocol whereby the temperature is stepped down by ~5°C either from a baseline of 25°C or, alternatively, from a "hot" baseline of 30°C. In this set-up, we expect that cells responding to absolute cold (rather than cooling) would only respond to the stimulus starting at the 25°C baseline and dipping into temperatures that are below the fly's favorite range (i.e. "cold" temperatures).

To test for temperature responses, we again used two-photon calcium imaging, measuring calcium transients at the PAL terminals of each cell type by selective targeting of GCaMP. Our results clearly demonstrate that, while the calcium responses of all three cell types appear to have non-adapting components, only the chamber one sacculus neurons exclusively respond to cold, but not to cooling (Figure 3S–U).

Together with the results of connectivity experiments, this observation suggests that all three sensory cell types may contribute to shape TPN-II's responses to temperature, but that the "absolute" cold temperature signal recorded in TPN-IIs is contributed by chamber one neurons of the sacculus.

Interestingly, while calcium transients in the terminals generally correlate well with synaptic release, the activity recorded in TPN-IIs does not appear to be a simple summation of the activity of these pre-synaptic cell types, suggesting additional processing is likely to occur at this synapse.

TPN-IIs have selective targets in the fly brain

What is the behavioral significance of this persistent, "cold" temperature activity relayed by sensory neurons of the sacculus and prominently recorded in specialized second-order neurons of the thermosensory system?

While many second-order neurons of the thermosensory system (TPNs) share common higher brain targets (such as the calyx of the mushroom body, lateral horn and posterior lateral protocerebrum, [8, 9]), non-adapting TPN-IIs exclusively innervate a microglomerulus at the edge of the calyx [8](Figure 4A). We reasoned that this anatomy may underlie selective connectivity in the brain, and that revealing TPN-II's synaptic targets may illuminate circuits that utilize specifically cold temperature information to process behavior happening on slow timescales.

Therefore, we used two-photon guided conversion of photoactivatable GFP (PA-GFP [14]) to identify TPN-II's cellular targets. First, we engineered flies where PA-GFP was constitutively expressed throughout the brain (under the control of syb-Gal4), and the TPN-II terminals were selectively labelled by a red fluorescent protein (Figure 4B). Then, using the red fluorescence as a guide, we photo-converted PA-GFP exclusively in a volume tightly

overlapping the TPN-II axon terminals, and traced the labeled neurites of next-order neurons, as they became illuminated by diffusion of the photo-converted fluorophore (Figure 4C).

Our results reveal that prominent targets of R60H12 cold-activated TPNs are two distinctive neurons that have been previously described as components of the circadian network in the *Drosophila* brain (Figure 4C,D). The 1a cluster of "Dorsal Neurons" (DN1a) is part of a network of DNs that express key circadian gene products such as Clock and Period (Figure 4D–J). DN1as are defined by their unique anatomy (including projections to the accessory medulla) and by the fact that they are among a small group of DN1s which express Cryptochrome ([15], Figure 4K–M). Importantly, DN1as are indeed direct synaptic targets of TPN-IIs, as demonstrated by synaptic GRASP (Figure 4N,O).

DN1a neurons are directly inhibited by TPN-IIs in cold conditions

What is the effect of cold temperature on DN1a activity? Given TPN-II's firing rates are elevated in cold conditions and scale proportionally with cold temperature, we expected TPN-IIs to drive similar activity in the post-synaptic DN1as. Instead, cold temperature all but shut down activity in this cell type (Figure 5A–C).

Using temperature steps of different magnitude (and patch-clamp electrophysiology as described above), we observed that a cooling step as small as 2°C was sufficient to nearly silence DN1as (from an initial baseline of nearly 10Hz), and that the firing of this cell type was essentially completely silenced at temperatures 4 or 6°C below the 25°C baseline (Figure 5D–E). As expected, and consistent with the properties of TPN-IIs, DN1a's inhibition by cold temperature was very persistent (showing limited recovery in stable cold conditions) and depended on the presence of the antennae (Figure S3).

In contrast to strong responses to cold, DN1as demonstrated little persistent modulation by heat (i.e., when the temperature was stepped above the 25°C range, Figure 5D,F). This is again consistent with the limited response recorded from TPN-IIs in the hot range. Interestingly, we did observe a rapid, heating-induced burst in DN1a firing that could not be directly correlated with the responses of the pre-synaptic TPN-IIs (Figure 5D and compare with Figure 1F,G). This observation suggests an additional (albeit transient) heating-evoked drive to DN1a.

The fact that DN1as are powerfully silenced (rather than activated) by cold temperature, and at the same time are synaptic targets of cold-activated TPN-IIs, suggests that TPN-IIs may be inhibitory projection neurons. Indeed, immunohistochemistry demonstrated that TPN-IIs express the inhibitory neurotransmitter GABA (Figure 5G), and bath-application of the $GABA_A$-receptor antagonist Picrotoxin abolished cold-inhibition of DN1as (Figure 5H–J).

Together, our results suggest that cold-activated TPN-IIs directly inhibit the activity of the clock neuron cluster DN1a, through a GABA-ergic synapse, in cold conditions. Because clock neurons can exhibit endogenous (clock-regulated) rhythms in activity, we next tested the possibility that activity rhythms may also shape the firing profile of DN1as, perhaps gating the effect of cold temperature on DN1a activity.

DN1as have clock-regulated rhythms in activity, but are invariably inhibited by cold

Previous work has demonstrated that “posterior” DN1s (DN1ps) possess endogenous mechanisms to modulate firing rates in a time-of-day dependent fashion [16]. To test if DN1as may display similar properties, we recorded their activity at different times of day and night. Our recordings suggest that, as for DN1ps, DN1as also possess time-of-day dependent modulation, with higher firing rates during the first part of the day (ZT0–4, ~12Hz) as compared to the last time point of the night (ZT20–24, ~6Hz; Figure 5K). These activity rhythms are present in both females and males (Figure 5K,L), and are regulated by the molecular clock, as they were abolished in per^{01} mutants (Figure 5L). Higher rates of DN1a firing in the morning may reflect an important role for these cells in the regulation of morning activity and/or in the night-to-day sleep/wake transition. Interestingly, notwithstanding these rhythms of activity, cold steps of 4° or 6°C (from a baseline of 25°C) were effective in significantly reducing DN1a activity at all time points tested (Figure 5M,N). Hence, in the absence of other external stimuli, cold temperature should be effective in silencing DN1a activity at all times of day and night.

Cold temperature has both an acute and persistent effect on fly activity and sleep

What is the functional significance of this powerful cold-inhibition of DN1a? The posterior cluster of DN1s (DN1ps) has been abundantly implicated in the regulation of sleep, including the onset and extent of the afternoon “siesta” flies enjoy in hot days [17–19], as well as the regulation of sleep patterns in cold days [20]. At least one previous publication suggests that DN1as may also be involved in the regulation of daytime sleep [21].

Here, our goal was to test the possibility that DN1as may be directly involved in the regulation of activity and sleep by temperature, and that their powerful inhibition by cold may be of significance for the regulation of activity/sleep patterns in persistent cold conditions. Unlike previous studies, our experiments could be guided by knowledge of the specific thermal range that modulates DN1a’s activity via connections with the antennal TRNs/TPN-II circuit (Figure 6).

At the normal rearing temperature of 25°C (and under 12hrs light : 12hrs dark, or LD, cycles) fly behavior is characterized by peaks of activity corresponding to the late night-early morning transition (“morning peak”) and to the end of the day (“evening peak”; see Figure 6A, gray bar graph). Fly sleep is generally defined as inactivity that persists for 5 minutes or longer [22, 23] and, as such, most of fly sleep occurs at night, yet flies (male flies in particular [24]) also display a prominent mid-day “siesta” (Figure 6A, black plot) - perhaps to avoid potentially hot/dry conditions in the mid-day [25].

Cold temperature (18°C) has both an acute and persistent effect on fly activity and sleep: cold conditions rapidly suppress morning activity (and increase morning sleep; Figure 6A, blue bar graphs and lines). Activity in the evening is also reduced, in addition, the onset of evening activity is advanced (arrow in bar graph, Figure 6A). The overall effect of cold on daytime sleep is that the “siesta” is advanced to earlier time points –potentially an adaptation to the fact that cooler conditions normally accompany the seasonal shortening of days (Figure 6A, blue plot; see also [26]).

Interestingly, this acute shift in siesta sleep can be ascribed to independent and reversible effects of cold temperature on sleep in the morning and evening: in LD conditions, a defined 3hrs cold step in the morning *increases* sleep (but, following return to 25°C, fly behavior returns to normal, Figure 6B), while a similar defined cold step in the evening *decreases* sleep (Figure 6C and see D for quantifications).

Silencing DN1a output mimics cold conditions

Are DN1as involved in the restructuring of daytime sleep in response to cold temperature? To test the potential involvement of DN1as (and TPN-IIs) in this process, we first developed genetic reagents to selectively target each cell type for genetic silencing. Starting from broader drivers, we created intersectional split-Gal4 lines narrowly active in either DN1as (Figure 6E) or non-adapting TPN-IIs (see Figure 3I and methods for details). Next, we used these drivers to express a transgenic blocker of synaptic transmission (Tetanus Toxin Light chain, [27]) and monitored the effect of this manipulation on sleep and activity.

Remarkably, genetic silencing of DN1a's output at 25°C partially mimicked cold conditions: under LD cycles, the onset of siesta sleep was advanced even at 25°C, resembling the response to cold conditions observed in controls (Figure 6G,H and see F,I for controls). This suggests that reducing the output of DN1as in the morning may be a key mechanism for daytime siesta sleep advancement by cold temperature. Interestingly, blocking DN1a's output also prevented the plastic remodeling of sleep by cold temperature in the evening (ZT6–12). This time, constitutive block of DN1a output produced a stable (i.e. temperature-independent) sleep profile more similar to the control's 25°C conditions, as DN1a>TNT flies did not reduce the amount of evening sleep in response to cold (Figure 6G,H).

As cold temperature suppresses DN1a firing in both morning and evening (Figure 5), this observation is incompatible with simple models in which silencing DN1a invariably results in more sleep, irrespective of time of day. Instead, our results suggest that the appropriate timing and extent of DN1a activity may be crucial for the dynamic regulation of daytime sleep patterns, and for their plastic adaptation to changes in the external temperature.

Next, we tested the potential impact of TPN-II silencing. Our previous results suggest that TPN-IIs provide powerful inhibitory drive to DN1as in cold conditions. Consistent with this, silencing TPN-II's output had no effect on sleep at 25°C. After a shift to 18°C, siesta sleep of TPN-II>TNT flies advanced normally. Interestingly, constitutive block of TPN-II's output again prevented sleep restructuring in the evening, producing a stable sleep profile similar to that of DN1a>TNT flies (Figure 6K,L and compare to G,H).

The fact that reducing the output of inhibitory neurons (TPN-IIs) had the same (rather than the opposite) effect on evening sleep to that obtained by silencing their targets (DN1as) is again consistent with the notion that the dynamics of DN1a activity (rather than their net output at a given time point) may be important to determine the appropriate pattern of daytime sleep, so that locking the system in one state may produce similar effects.

Notably, the overall daytime sleep profile of TPN-II>TNT flies at 18°C was remarkably similar to that of DN1a>TNT flies at 25°C (both in the morning and evening, compare

Figure 6K, blue plot with 6G, black plot). This daytime sleep profile may perhaps represent a default state of the system that results from manipulations that disconnect it from external temperature drive.

Despite this potentially complex interaction, our results suggest that the circuit composed of inhibitory TPN-IIs and DN1a plays a key role in mediating the restructuring sleep and activity patterns in cold conditions.

Dark and cold synergize to suppress morning wakefulness

In the environment, the seasonal arrival of cold temperatures is often accompanied with darker conditions and shorter days. Next, we tested the potential impact of light on DN1a function and fly behavior in the cold. Under light/dark cycles in constant cold (LD at 18°C), control flies robustly wake up at the first appearance of light (‘lights-on’), but quickly return to sleep within 60–90 minutes (Figure 6); our results also demonstrate that, at 25°C, blocking DN1a output significantly increases morning sleep partially mimicking cold conditions (Figure 6G,H). Interestingly, when switched to constant dark/cold conditions (DD at 18°C), control animals nearly fail to wake up in the morning altogether (Figure 7A, blue line, and see B for quantification). Blocking the output of DN1as mimics this effect of cold, so that -in the absence of a light signal-most DN1a>TNT flies fail to wake up in the morning even at 25°C (Figure 7C–E). Optogenetic activation of TPN-IIs was sufficient to reproduce this effect, generating animals that largely ignore the “light on” signal in the morning (Figure 7F–H; note that, in dark conditions, cold temperature also produces a significant increase in evening sleep, an effect reproduced by DN1a silencing and optogenetic activation of TPN-IIs, Figure 7F,G,I).

Hence, light and cold have powerfully antagonistic effects on morning wakefulness. Based on these results, we tested the interaction of light and temperature in regulating DN1a firing rates.

DN1as directly integrate light and cold temperature signals

Ample evidence suggests that DN1a activity may be directly or indirectly modulated by light. For example, DN1as express the blue light receptor Cryptochrome [15] and, in the larva, are known targets of light-responsive ventral Lateral Neurons (LNvs, a core component of the clock circuit) [28]. Importantly, the “small” LNvs, or sLNvs have been described as master regulators of morning activity [29] and have been suggested to form reciprocal connections with DN1as [21].

Our results suggest that indeed DN1as respond to light, as well as to sLNv signaling. First, we observed light responses in DN1a (Figure 7J–L, and see [29]). Next, we showed that “artificial” activation of sLNvs using P2X2 results in an increase of DN1a firing (Figure 7M,N). Finally, we recorded an increase in firing rates in DN1as upon focal application of the neuropeptide PDF (normally expressed by sLNvs [30]; and for which DN1as express the cognate receptor PDFR [31]; Figure 7Q,R).

Strikingly, light exposure, artificial sLNv activation, and PDF application were each able to partially overcome cold-inhibition of DN1as (Figure 7K,L,O,P,S,T), suggesting that light

and/or LNv signaling (through PDF release) could drive DN1as even in cold conditions, and explaining the dominant effect of light in setting the beginning of daytime activity.

Together, our results demonstrate functional connectivity between sLNvs and DN1as, and suggest that DN1a activity is shaped by signals from the circadian clock and modulated by the opposing pushes of light and cold temperature, dynamically shifting the pattern of daytime sleep to better adapt to changing environmental conditions.

DISCUSSION

In this work we uncover a complete circuit, from sensory neurons to circadian and sleep centers, that processes information about absolute cold temperature to exert influence on fly behavior in the timescale of minutes, to hours to days.

The circuit we describe is comprised of sensory neurons of the antenna (including newly identified thermosensory neurons only active in the cold) and of specialized second-order thermosensory projection neurons of the PAL, and provides persistent inhibition to the DN1a cluster of circadian neurons to adapt sleep/activity patterns specifically to cold conditions.

Our data show that “absolute temperature” and “temperature change” signals can be extracted by second order neurons from the activity of peripheral thermoreceptors and demonstrate that persistent signaling in sensory circuits mediates long-lasting changes in behavior, beyond the rapid responses that are generally well understood. Moreover, our results illustrate how the fly nervous system selectively encodes and relays absolute cold temperature information to adapt behavior specifically to cold conditions.

What may be the significance of this sensory mechanism for the animal’s natural behavior? Thermal conditions are well-known to exert long-lasting changes in physiology and behavior, but due to the pervasive nature of temperature itself, such changes do not necessarily require input from a sensory circuit. For example, on the time scale of days and weeks, cold temperature promotes the alternative splicing of clock genes [26, 32], directly affecting the dynamics of the molecular clock. The sensory mechanism we discover here allows the animal to respond both rapidly and persistently to cold conditions. Such a mechanism may be important to bridge the gap between behavioral responses on the time scale of minutes to hours, and biochemical changes that may take days to fully set-in (and may be difficult to reverse).

In a small poikilotherm, “cold” (the range of temperature below the optimal species-specific value determined by the biochemistry of the animal) profoundly impacts motility and the ability to process stimuli. Cold temperature can quickly render a fly unable to move rapidly or fly away [33], and it is well known that larger insects such as bumble bees have evolved adaptations to ensure that their internal temperature is sufficient to support flight once they leave the hive [34]. We speculate that, for example, it may be adaptive for a fly to “sleep in” on a cold, dark morning until the conditions are met for it to warm up sufficiently as to rapidly avoid predation. If cold conditions indeed persist, the new sleep/wake pattern may become further reinforced by stable biochemical/molecular changes and become part of a new seasonal pattern of activity.

Following up on the TPN-II targets, our work also identifies DN1a neurons as a key node for the integration of sensory information with internally regulated drives for rest and activity. We show that DN1as are powerfully and persistently inhibited by cold temperature, but also that they have clock-regulated rhythms of activity, respond to light, and receive excitatory drive from sLNvs (which are part of the endogenous pacemaker and are in turn also activated by light [35]). Together, our results demonstrate how information about external conditions (light and temperature) is directly relayed to a circadian/sleep center in the brain and integrated with internal drives to adapt sleep and wake cycles to changing external conditions.

Our results open a window on the temporal structure of sensory signaling in the fly thermosensory system and reveal how -even within sensory modality-distinct neural circuits can operate on different temporal scales to drive appropriate behavioral responses.

STAR METHODS

Lead Contact—Further information and requests for reagents should be directed to and will be fulfilled by the Lead Contact, Marco Gallio (marco.gallio@northwestern.edu).

Materials Availability—This study did not generate new unique reagents. Requests of fly stocks should be directed to and will be fulfilled by the Lead Contact, Marco Gallio (marco.gallio@northwestern.edu).

EXPERIMENTAL MODEL AND SUBJECT DETAILS

Fly Strains—*Drosophila melanogaster* strains were reared on cornmeal agar medium under 12:12 LD cycles at 25°C. Stocks were obtained from Bloomington Drosophila Stock Center (BDSC) or Vienna Drosophila Resource Center (VDRC). The following stocks were used: IR25a Gal4 (BDSC 41728), R49B06 Gal4 (BDSC 50409), R49B06 LexA (BDSC 52707), R25B07 AD (BDSC 70144), R25B07 LexA (BDSC 54125), R77C10 Gal4 (BDSC 39958), R77C10 DBD (BDSC 69705), R60H12 AD (BDSC 70761), VT032805 DBD (BDSC 75119), R49A06 Gal4 (BDSC 50401), VT003226 Gal4, R23E05 Gal4 (BDSC 49029), R23E05 AD (BDSC 70601), R92H07 DBD (BDSC 70004), 20XUAS-IVS-GCaMP6f (BDSC 42747), 20XUAS-IVS-jGCaMP7f (BDSC 79031), 20XUAS-IVS-CsChrimson.mVenus (BDSC 55135), 13XLexAop-IVS-jGCaMP7f (BDSC 80914),13XLexAop-TdTomato, UAS-C3PA, UAS-SPA and synaptobrevin-Gal4 (kind gifts from V. Ruta and B. Noro), AOP.Syb:spGFP[1–10],UAS.spGFP[11] (BDSC 64315) PDF-LexA and Per^{01} (kind gifts of R. Allada), AOP-P2X2 (kind gift of O. Shafer), 10XUAS-IVS-mCD8::GFP (BDSC 32186) UAS-TNT (kind gift from M. Rosbash). A full description of genotypes used in each figure can be found in Table S1. Male flies were used for all behavioral experiments. In Figure 5, electrophysiological recordings were performed on males and females, separately, as indicated; all other recordings were performed on males. A full description of genotypes used in each figure can be found in Table S1. A full list of fly lines can be found in the Key Resources Table.

METHOD DETAILS

Characterization of Gal4, LexA and split-Gal4 drivers—In addition to saccuclus chamber I neurons, R25B07-LexA expresses in the lateral horn, subesophageal ganglia, and a single olfactory glomerulus in the antennal lobe. R77C10-Gal4 is active in arista cold cells, the ACc, and subesophageal ganglia. IR25a-Gal4 expresses in ACc, and a detailed description of antennal sensory neurons in this line can be found in Enjin et al., 2016. R25B07 AD ∩ R77C10 DBD is active in 2–3 cold cells of the arista. R60H12 AD ∩ VT032805 DBD expresses in TPN-IIs, weakly in subesophageal ganglia, and a pair of cells in the ventral nerve cord. R92H07 AD ∩ R23E05 DBD is active in DN1as and no other neurons in the brain.

Electrophysiology—Whole-cell patch clamp electrophysiology experiments were performed on 2–3 days old flies. Flies (generally females, except for per^{01} mutants and controls) were anaesthetized by brief cold exposure in an ice bath (~0°C) for ~1 min. Using a dissection microscope (Nikon SMZ1000), a small window in the head cuticle was opened and the underlying perineural sheath was gently removed using fine forceps (Moria Surgical). Brain tissue was exposed while maintaining connectivity with peripheral antennae, and bathed in artificial hemolymph (AHL) solution containing the following (in mM): 103 NaCl, 3 KCl, 26 NaHCO3, 1 NaH2PO4, 8 trehalose dihydrate, 10 dextrose, 5 TES, 4 MgCl2, adjusted to 270–275 mOSm. For experiments, 1.5 mM CaCl2 was included and the solution was continuously bubbled with 95% O2 5% CO2 to pH 7.3 and perfused over the brain at a flow rate of 1–2 mL/min. To target neurons for patching under the 2-photon microscope, Gal4 lines expressing GFP for neuron targeting were excited at 840 nm and detected using a photomultiplier tube (PMT) through a bandpass filter (490–560 nm) using an Ultima 2-photon laser scanning microscope (Bruker, formerly Prairie Technologies). The microscope is equipped with galvanometers driving a Coherent Chameleon laser and a Dodt detector was used to visualize neural tissue/somata. Images were acquired with an upright Zeiss Examiner.Z1 microscope with a Zeiss W Plan-Apochromat 40×0.9 numerical aperture water immersion objective at 512 pixels × 512 pixels resolution using PrairieView software v. 5.2 (Bruker). Current clamp recordings were performed with pipettes pulled (Sutter P-97) using borosilicate capillary tubes (WPI Cat # 1B150F-4) with open tip resistances of 20 +/− 3 MΩ filled with internal solution containing the following (in mM): 140 K-aspartate, 1 KCl, 1 EGTA, 10 HEPES, 4 Mg-ATP, 0.5 Na3-GTP, pH 7.3, 265 mOsm. To visualize the electrode and fill the cell after recording to confirm GFP co-localization, Alexa Fluor 594 Hydrazide (5 μM; Thermofisher Scientific Cat. # A10438) was added into the intracellular solution, excited using the 2-photon microscope at 840 nm, and detected with a second PMT through a bandpass filter (580–630 nm). Recordings were made using Axopatch 200B patch-clamp amplifier and CV203BU headstage (Axon Instruments), lowpass filtered at 2 KHz, scaled to a 20x output gain, digitized with a Digidata 1320 A, and acquired with Clampex software v.9.2.1.9 (Axon Instruments).

Temperature stimulation: For temperature stimulation, preparations were continuously perfused with Ca^{2+}-containing AHL (as described above). AHL was gravity fed through a 3-way valve (Lee company, part # LHDA1231315H) and flow rate was adjusted through a

flow regulator. Following the valve, temperature was precisely regulated through 2 in-line solution heater/coolers (Warner, cat. # SC-20) in parallel with by a dual channel bipolar temperature controller (Warner Instruments, Cl-200A). Excess heat produced by each SC-20 Peltier was dissipated through a liquid cooling system (Koolance, Cat. # EXT-1055). To circumvent changes in resistivity and voltage offsets from changing the temperature of the bathing solution, the reference Ag-Cl pellet electrode was placed in an isolated well adjacent to the recording chamber (Warner Instruments, Cat. # RC-24N), filled with identical AHL and connected via a borosilicate capillary tube filled by 2% agar in 3 M KCl. The bath temperature was precisely recorded using a custom Type T thermocouple with 1cm exposed tip (Physitemp, Cat. # T-384A) connected to a thermometer (BAT-12, Physitemp) with an analogue output connected to the digitizer and sampled at 10 kHz. The tip of thermocouple was threaded through a borosilicate capillary tube and precisely placed near the antennae using a micromanipulator (MP-225, Sutter Instruments).

Time of Day Electrophysiology Experiments: Flies were reared on a 12:12 L:D cycle at 25°C. Experiments were performed on female flies 2–3 days post-eclosion and recordings were binned in 4 hr intervals according to Zeitgeber Time (ZT). For ZT0–12 recordings a white LED was used during the dissection, whereas during ZT 12–24, red light was used instead in otherwise complete darkness. The baseline firing rate was established and taken from an average of the firing rate in the first 1–2 min after break-in and the establishment of whole cell configuration. Mean firing rate (Hz) ± SD are reported for each bin. An unpaired 1-tailed t-test was used to test for significant differences in firing rate between night (ZT 20–24) and day (ZT 0–4). For experiments in a per^{01} background, Gal4 lines expressing GFP were crossed to female per^{01}; as *per* maps to the X chromosome, only male progeny were used for experiments.

Light stimulation: Flies were reared on a 12:12 L:D cycle at 25°C and dissected using white light. Experiments were performed on female flies 2–3 days post-eclosion at ZT 0–8 with intact eyes. Whole cell recordings were established using 2-photon illumination at 840 nm. Flies were then left in darkness at 25°C until stimulated from below using the microscope condenser halogen lamp (Sunlite Q100). A light intensity of ~430 lux was measured through the recording chamber using a Digital lux meter (# LX1330B, Dr. Meter). Flies were then cooled to 20°C for several minutes and then stimulated again with the condenser light. To quantify the change in firing rate from light stimulation, a baseline period of ~30s was averaged and compared to the peak response elicited upon light exposure.

Pressure ejection of chemicals: For focal application of ATP (20 mM in AHL) or PDF peptide (50 μM in AHL, GenScript), solutions were backfilled into a borosilicate capillary tube (WPI) connected to a TTL-triggerable PV830 Pneumatic PicoPump (WPI). Alexa 594 Hydrazide (5 μM) was included to confirm and record the fluorescence intensity and time course of the ejected solution. Pipettes were pulled using a P-97 puller (Sutter) to open tip resistances of 5–10 MΩ and precisely positioned using a micromanipulator (Sutter MP-225) near DN1a projections. Constant pressure (5 psi) was maintained for the duration of the stimulus. For ATP experiments, controls were performed in Gal4 lines expressing GFP only.

Immunohistochemistry—Staining of fly brains was performed essentially as previously described (Gallio et al., 2011). Briefly, brains of young (3–5d old) male and female flies were dissected in cold PBS or artificial hemolymph and fixed in 4% PFA. Blocking was performed in PBSBT (PBS, 0.2% Triton X-100, 3% BSA) and samples were incubated overnight at 4°C with the appropriate dilution of primary antibody in PBSBT. The following day, samples were washed and incubated for 3hr with fluorescently tagged secondary antibody diluted to the appropriate concentration in PBSBT. The following antibodies were used: chicken anti-GFP (Abcam #ab13970), rabbit anti-dsRED (Clontech #632496), rabbit anti-GABA (1:200, Sigma #A2052), goat anti-CLK (dC-17) (1:500, Santa Cruz Biotechnology #sc-27070), rabbit anti-Per (1:5000, a gift from the Allada lab), rabbit anti-Cry (1:50, a gift from the Allada lab [36], donkey anti-chicken Alexa 488 (1:250, Jackson ImmunoResearch #703-545-155), donkey anti-rabbit Alexa 594 (1:250, Jackson ImmunoResearch #711-586-152), donkey anti-goat Alexa 568 (1:250, Invitrogen #A-11057). For staining of antennal nerves to characterize ACc, the following antibodies were used: rat anti-Elav (1:50, Hybridoma Bank #Rat-Elav-7E8A10 anti-elav), goat anti-rat DyLight 594(1:500, NovusBio #NBP1–76096), mouse anti-Repo (1:50, Hybridoma Bank #8D12 anti-Repo), donkey anti-mouse Alexa 594 (1:500, Abcam #ab150105), chicken anti-GFP (1:500 Abcam #ab13970), donkey anti-chicken Alexa 488 (1:500, Jackson ImmunoResearch #703-545-155).

Fluorescence Microscopy and Image Analysis—Confocal imaging of antennae and immunofluorescent-stained brains was performed on a Zeiss LSM 510 confocal microscope equipped with Argon 450–530nm, Helium-Neon 543nm, and Helium-Neon 633 nm lasers and a Zeiss LCI Plan-Neofluar/0.8 DIC Imm Corr 25x objective at 512×512 pixel resolution. Two-photon imaging of GFP-, TdTomato-, and sybGRASP-labeled neurons was performed on a Prairie Ultima two-photon microscope with a Coherent Chameleon Ti:Sapphire laser tuned to 945nm, GaAsP PMTs and an Olympus 40X 0.9NA water immersion objective at 512×512 pixel resolution and 1X or 2X optical zoom. Maximum projections were obtained from stacks taken at 1 μm steps. Images were processed in Fiji.

Antennae Anatomy—Large online collections of Gal4 driver lines (Janelia Farm FlyLight initiative, Vienna Drosophila Resource Center ViennaTile) were visually screened to identify driver lines putatively active in sensory neurons innervating the PAL. Drivers were crossed to 10XUAS-IVS-mCD8::GFP and the antennae of the resulting progeny examined under confocal microscopy. Antennae of young flies were dissected and collected in cold artificial hemolymph and mounted in artificial hemolymph or Vectashield.

Ablation of Antennae—Male and female flies were collected shortly after eclosion and anesthetized on ice, fine forceps were used to gently pluck the antennae from the flies. Removal of the entire third segment and arista was confirmed visually. Imaging experiments in the PAL were conducted 7–10 days post-ablation.

Calcium Imaging—Calcium imaging of temperature stimuli was performed essentially as previously described (Gallio et al. 2011; Frank et al., 2015). Gal4 driver line males were crossed to virgin GCaMP females (see STAR Methods Key Resource Table for a complete

list of genotypes) and progeny used for imaging experiments 3–5 days post-eclosion. Dissections and temperature stimuli were performed as described above in AHL continuously bubbled with 95% O2 5% CO2. Images were acquired at 256×256 or 512×512 pixels resolution at a rate of 4 Hz on a Prairie Ultima two-photon microscope with a Coherent Chameleon Ti:Sapphire laser tuned to 945nm.

Circadian Behavioral Experiments—All flies were reared at 25°C in 12 hr light: 12 hr dark (LD) conditions. Male flies (3–5 days old) were loaded into 65mm × 5mm tubes containing 5% sucrose 2% agar food medium. Locomotor activity was recorded using the Drosophila Activity Monitoring System (DAMS, Trikinetics) in 1 minute intervals. Temperature, light and humidity were controlled using a DR-36NL incubator (Percival Scientific). To suppress synaptic output of DN1a split Gal4 (R23E05 AD ∩ R92H07 DBD) and TPN-II split Gal4 (R60H12 AD ∩ VT032805 DBD), males were crossed to virgin UAS-TNT females, and male progeny were assayed.

Optogenetic Stimulation: All-*trans* retinal powder (RET, Sigma-Aldrich) was mixed with ethanol to prepare a 100mM stock solution. 1mL of stock was then mixed with 250mL of molasses and cornmeal medium to produce 400μM food. Flies were reared on this medium, and then transferred to 400μM retinal 5% sucrose 2% agar medium for data collection using the DAMS. Control food was prepared using the same volume of ethanol. To optogenetically activate TPN-II, TPN-II split Gal4 (R60H12 AD ∩ VT032805 DBD) males were crossed to virgin UAS-CsChrimson females, and male progeny were assayed in a DigiTherm incubator (Trikinetics). For time-delimited optogenetic activation (i.e. to miminize CsChrimson activation by the standard white incubator light), we covered the light tubes with ~488 nm polyester film (Rosco #R375) to produce 210 lux blue light. Flies were reared on blue light 12:12 LD cycles at 25°C and behavior was assayed in the same incubator. For sleep analysis (Fig. 7 G–I), flies were entrained to blue-LD cycles for 4 days, with red light stimulation from ZT0–3 on day 2, and ZT6–12 on day 4. Constant red light (4800 lux) was produced using 3 symmetrically-placed high-power 660nm LEDs (M660L3 or M660L4, Thorlabs) mounted on heat sinks. The angle and height of the LEDs were adjusted to ensure uniform illumination. Lux measurements were made using a Digital lux meter (# LX1330B, Dr. Meter).

QUANTIFICATION AND STATISTICAL ANALYSIS

Detection of Action Potentials—Membrane potential recordings were made in current clamp mode sampled at 10 kHz. Data was analyzed offline using Axograph and Igor Pro. Action potentials (spikes) were detected using custom scripts in Igor Pro using Neuromatic v2.6i plug-in [37]. A first derivative transformation was performed on the membrane potential trace defining dV/dt. Then a constant dV/dt threshold was used to detect individual spikes. Peristimulus time histograms (PTH) of firing rate were made by binning detected spikes in 1 second bins, defining spikes/s (Hz). In experiments in which single trials from individual cells were averaged, the line and shading indicate the mean firing rate (Hz) ± SD. For experiments in which multiple sweeps were performed at a given stimulus temperature, average PTH were calculated per cell; the line and shading indicate the mean firing rate (Hz) ± SD; then across cells the line and shading indicate the mean firing rate (Hz) ± SEM. For

figure panels using pseudocolored histograms to show firing rates for extended temperature stimuli, an image matrix representing the firing rates (in 1 s bins) was imported into ImageJ.

Temperature—In experiments in which single trials from individual cells were averaged, the line and shading indicate the mean temperature (°C) ± SD. For experiments in which multiple sweeps were performed at a given stimulus temperature, the line and shading indicate the mean temperature (°C) ± SD across cells. To test for a significant relationship between temperature and firing rate for TPN-II, a f-test was performed and significance (*) defined as $p < 0.05$.

Time of Day Cellular Effects—An unpaired 1-tailed t-test was used to test for significant differences in firing rate between night (ZT 20–24) and day (ZT 0–4) for WT or *per*^{01} flies. A paired 1-tailed t-test was used to test for significant decreases in firing rate of different magnitude cooling steps between night (ZT 20–24) and day (ZT 0–4). Significance (*) was defined as $p < 0.05$.

Cellular Effects of Light—A paired, 1-tailed t-test was used to test for significant differences in firing rate between darkness and light conditions, both at 25°C and then at 20°C.

Pressure Ejected Chemicals—PTHs were calculated and the lines and shading represent the mean firing rate ± SEM. To confirm statistical significance between baseline firing and baseline + ATP/PDF, a paired 1-tailed t-test was used and significance (*) defined as $p < 0.05$.

Calcium Imaging—Delta F/F analysis was carried out using custom MAT LAB scripts. To calculate change in fluorescence we used the formula Delta $F/F_0 = (F_t\text{-}F_0)/F_0$, where F_0 is the baseline fluorescence determined by averaging frames before stimulus onset and F_t is the fluorescent value at a given time. Circular regions of interest (ROIs) of constant area were drawn manually, as appropriate, using the overlaid averaged image as a guide. Representative stimulus and Delta F/F response pairs were used to generate average traces in MATLAB. Values across individual trials were averaged and the standard deviation was determined for each time point.

Circadian Behavior—Sleep was defined as ≥5 consecutive minutes of inactivity. Activity and sleep analysis was performed using MatLab 2016a software (Mathworks). Sleep is displayed in 30 minute bins represented as mean ±SEM. For 25°C-18°C behavior comparisons, (Fig. 6 A, D, F–L), flies were entrained for 4 days to 12:12 LD at 25°C, then gradually transferred to 18°C during the 4th night (9 hr −0.8°C/hr linear cooling ramp, ZT12–21) for 3 additional days. 25°C activity and sleep data are the mean of 2 days before cooling, and 18°C data are the mean of 2 days after cooling. For cold step experiments (Fig. 6 B,C,D), flies were entrained in 12:12 LD at 25°C for 3 days. On the subsequent day, the temperature was stepped to 18°C from ZT 0–3 (0.35°C/min); after a day of recovery, the temperature was stepped to 18°C from ZT 6–12 (0.35°C/min). Quantifications are made between the pulse day and the preceding non-pulse day at 25°C. To test for significance differences of both sleep and activity at 25°C vs 18°C (Fig. 6 A–D, F–L), two-sided paired *t*-

tests were used. When comparing sleep across genotypes (Fig. 6 H, L), statistical significance was determined using a 2-way Analysis of Variance (ANOVA) with a post-hoc Bonferroni test for multiple comparisons. For Fig. 7 A–E, flies were entrained for 3 days 12:12 LD at 25°C, then transferred to constant darkness (DD) for one day at 25°C, or transferred to DD following a 9hr cooling ramp to 18°C (−0.8°C/hr). Because comparisons were made from different cohorts of flies (Fig. 7 A, B), two-sided unpaired *t*-tests were used to test for significance differences in sleep. When comparing sleep across genotypes (Fig. 7 D, E), statistical significance was determined using a 2-way Analysis of Variance (ANOVA) with a post-hoc Bonferroni test for multiple comparisons. For optogenetic experiments, a two-sided unpaired *t*-test was used to test for significant differences in sleep between RET+ vs RET− flies (Fig. 7 G–I).

Data and Code Availability—All data is available in the main text or the supplementary materials. Further information and requests for data and code should be directed to and will be fulfilled by the Lead Contact, Marco Gallio (marco.gallio@northwestern.edu).

Supplementary Material

Refer to Web version on PubMed Central for supplementary material.

ACKNOWLEDGMENTS

We thank Eilene Ni and David Kocoj for technical assistance, Evdokia Menelaou for help with spike analysis, Graham Robinson for graphical abstract artwork. Lindsey Macpherson, Tiffany Schmidt, Bridget Lear, Clark Rosensweig and members of the Gallio Lab for comments on the manuscript. Work in the Gallio lab is supported by NIH grant R01NS086859, a Pew Scholars Program in the Biomedical Sciences and a McKnight Technological Innovations in Neuroscience Awards (to M.G). M.A. was supported by training grant T32HL007909, D.F was supported by F31NS093873.

REFERENCES

1. (1842). Handworterbuch der Physiologie: 1, (Friedrich Vieweg und Sohn).
2. Hensel H, and Zotterman Y (1951). The persisting cold sensation. Acta Physiol Scand 22, 106–113. [PubMed: 14933133]
3. Hensel H (1974). Thermoreceptors. Annual Review of Physiology 36, 233–249.
4. Yarmolinsky DA, Peng Y, Pogorzala LA, Rutlin M, Hoon MA, and Zuker CS (2016). Coding and Plasticity in the Mammalian Thermosensory System. Neuron 92, 1079–1092. [PubMed: 27840000]
5. Ran C, Hoon MA, and Chen X (2016). The coding of cutaneous temperature in the spinal cord. Nat Neurosci 19, 1201–1209. [PubMed: 27455110]
6. Gallio M, Ofstad TA, Macpherson LJ, Wang JW, and Zuker CS (2011). The coding of temperature in the Drosophila brain. Cell 144, 614–624. [PubMed: 21335241]
7. Budelli G, Ni L, Berciu C, van Giesen L, Knecht ZA, Chang EC, Kaminski B, Silbering AF, Samuel A, Klein M, et al. (2019). Ionotropic Receptors Specify the Morphogenesis of Phasic Sensors Controlling Rapid Thermal Preference in Drosophila. Neuron 101, 738–747 e733. [PubMed: 30654923]
8. Frank DD, Jouandet GC, Kearney PJ, Macpherson LJ, and Gallio M (2015). Temperature representation in the Drosophila brain. Nature 519, 358–361. [PubMed: 25739506]
9. Liu WW, Mazor O, and Wilson RI (2015). Thermosensory processing in the Drosophila brain. Nature 519, 353–357. [PubMed: 25739502]
10. Enjin A, Zaharieva EE, Frank DD, Mansourian S, Suh GS, Gallio M, and Stensmyr MC (2016). Humidity Sensing in Drosophila. Curr Biol 26, 1352–1358. [PubMed: 27161501]

11. Frank DD, Enjin A, Jouandet GC, Zaharieva EE, Para A, Stensmyr MC, and Gallio M (2017). Early Integration of Temperature and Humidity Stimuli in the Drosophila Brain. Curr Biol 27, 2381–2388 e2384. [PubMed: 28736172]
12. Hamada FN, Rosenzweig M, Kang K, Pulver SR, Ghezzi A, Jegla TJ, and Garrity PA (2008). An internal thermal sensor controlling temperature preference in Drosophila. Nature 454, 217–220. [PubMed: 18548007]
13. Macpherson LJ, Zaharieva EE, Kearney PJ, Alpert MH, Lin TY, Turan Z, Lee CH, and Gallio M (2015). Dynamic labelling of neural connections in multiple colours by trans-synaptic fluorescence complementation. Nature communications 6, 10024.
14. Datta SR, Vasconcelos ML, Ruta V, Luo S, Wong A, Demir E, Flores J, Balonze K, Dickson BJ, and Axel R (2008). The Drosophila pheromone cVA activates a sexually dimorphic neural circuit. Nature 452, 473–477. [PubMed: 18305480]
15. Benito J, Houl JH, Roman GW, and Hardin PE (2008). The blue-light photoreceptor CRYPTOCHROME is expressed in a subset of circadian oscillator neurons in the Drosophila CNS. J Biol Rhythms 23, 296–307. [PubMed: 18663237]
16. Flourakis M, Kula-Eversole E, Hutchison AL, Han TH, Aranda K, Moose DL, White KP, Dinner AR, Lear BC, Ren D, et al. (2015). A Conserved Bicycle Model for Circadian Clock Control of Membrane Excitability. Cell 162, 836–848. [PubMed: 26276633]
17. Guo F, Yu J, Jung HJ, Abruzzi KC, Luo W, Griffith LC, and Rosbash M (2016). Circadian neuron feedback controls the Drosophila sleep--activity profile. Nature 536, 292–297. [PubMed: 27479324]
18. Lamaze A, Ozturk-Colak A, Fischer R, Peschel N, Koh K, and Jepson JE (2017). Regulation of sleep plasticity by a thermo-sensitive circuit in Drosophila. Sci Rep 7, 40304. [PubMed: 28084307]
19. Parisky KM, Agosto Rivera JL, Donelson NC, Kotecha S, and Griffith LC (2016). Reorganization of Sleep by Temperature in Drosophila Requires Light, the Homeostat, and the Circadian Clock. Curr Biol 26, 882–892. [PubMed: 26972320]
20. Yadlapalli S, Jiang C, Bahle A, Reddy P, Meyhofer E, and Shafer OT (2018). Circadian clock neurons constantly monitor environmental temperature to set sleep timing. Nature 555, 98–102. [PubMed: 29466329]
21. Fujiwara Y, Hermann-Luibl C, Katsura M, Sekiguchi M, Ida T, Helfrich-Forster C, and Yoshii T (2018). The CCHamide1 Neuropeptide Expressed in the Anterior Dorsal Neuron 1 Conveys a Circadian Signal to the Ventral Lateral Neurons in Drosophila melanogaster. Front Physiol 9, 1276. [PubMed: 30246807]
22. Hendricks JC, Finn SM, Panckeri KA, Chavkin J, Williams JA, Sehgal A, and Pack AI (2000). Rest in Drosophila is a sleep-like state. Neuron 25, 129–138. [PubMed: 10707978]
23. Shaw PJ, Cirelli C, Greenspan RJ, and Tononi G (2000). Correlates of sleep and waking in Drosophila melanogaster. Science 287, 1834–1837. [PubMed: 10710313]
24. Huber R, Hill SL, Holladay C, Biesiadecki M, Tononi G, and Cirelli C (2004). Sleep homeostasis in Drosophila melanogaster. Sleep 27, 628–639. [PubMed: 15282997]
25. Chen WF, Low KH, Lim C, and Edery I (2007). Thermosensitive splicing of a clock gene and seasonal adaptation. Cold Spring Harb Symp Quant Biol 72, 599–606. [PubMed: 18419319]
26. Majercak J, Sidote D, Hardin PE, and Edery I (1999). How a circadian clock adapts to seasonal decreases in temperature and day length. Neuron 24, 219–230. [PubMed: 10677039]
27. Sweeney ST, Broadie K, Keane J, Niemann H, and O'Kane CJ (1995). Targeted expression of tetanus toxin light chain in Drosophila specifically eliminates synaptic transmission and causes behavioral defects. Neuron 14, 341–351. [PubMed: 7857643]
28. Collins B, Kane EA, Reeves DC, Akabas MH, and Blau J (2012). Balance of activity between LN(v)s and glutamatergic dorsal clock neurons promotes robust circadian rhythms in Drosophila. Neuron 74, 706–718. [PubMed: 22632728]
29. Stoleru D, Peng Y, Agosto J, and Rosbash M (2004). Coupled oscillators control morning and evening locomotor behaviour of Drosophila. Nature 431, 862–868. [PubMed: 15483615]

30. Helfrich-Forster C (1995). The period clock gene is expressed in central nervous system neurons which also produce a neuropeptide that reveals the projections of circadian pacemaker cells within the brain of Drosophila melanogaster. Proc Natl Acad Sci U S A 92, 612–616. [PubMed: 7831339]

31. Shafer OT, Kim DJ, Dunbar-Yaffe R, Nikolaev VO, Lohse MJ, and Taghert PH (2008). Widespread receptivity to neuropeptide PDF throughout the neuronal circadian clock network of Drosophila revealed by real-time cyclic AMP imaging. Neuron 58, 223–237. [PubMed: 18439407]

32. Martin Anduaga A, Evantal N, Patop IL, Bartok O, Weiss R, and Kadener S (2019). Thermosensitive alternative splicing senses and mediates temperature adaptation in Drosophila. Elife 8.

33. Lehmann FO (1999). Ambient temperature affects free-flight performance in the fruit fly Drosophila melanogaster. J Comp Physiol B 169, 165–171. [PubMed: 10335614]

34. Heinrich B (1972). Energetics of temperature regulation and foraging in a bumblebee,Bombus terricola kirby. Journal of comparative physiology 77, 49–64.

35. Li MT, Cao LH, Xiao N, Tang M, Deng B, Yang T, Yoshii T, and Luo DG (2018). Hub-organized parallel circuits of central circadian pacemaker neurons for visual photoentrainment in Drosophila. Nature communications 9, 4247.

36. Rush BL, Murad A, Emery P, and Giebultowicz JM (2006). Ectopic CRYPTOCHROME renders TIM light sensitive in the Drosophila ovary. J Biol Rhythms 21, 272–278. [PubMed: 16864647]

37. Rothman JS, and Silver RA (2018). NeuroMatic: An Integrated Open-Source Software Toolkit for Acquisition, Analysis and Simulation of Electrophysiological Data. Front Neuroinform 12, 14. [PubMed: 29670519]

Highlights

- The fly antenna contains 3 types of cold-activated sensory neurons
- Cold cells converge on “cold” domain of the brain thermosensory map
- Second-order TPN-IIs relay absolute cold, below *D. melanogaster*’s favorite 25°C
- TPN-IIs inhibit DN1a circadian neurons, adapting sleep to cold/dark conditions

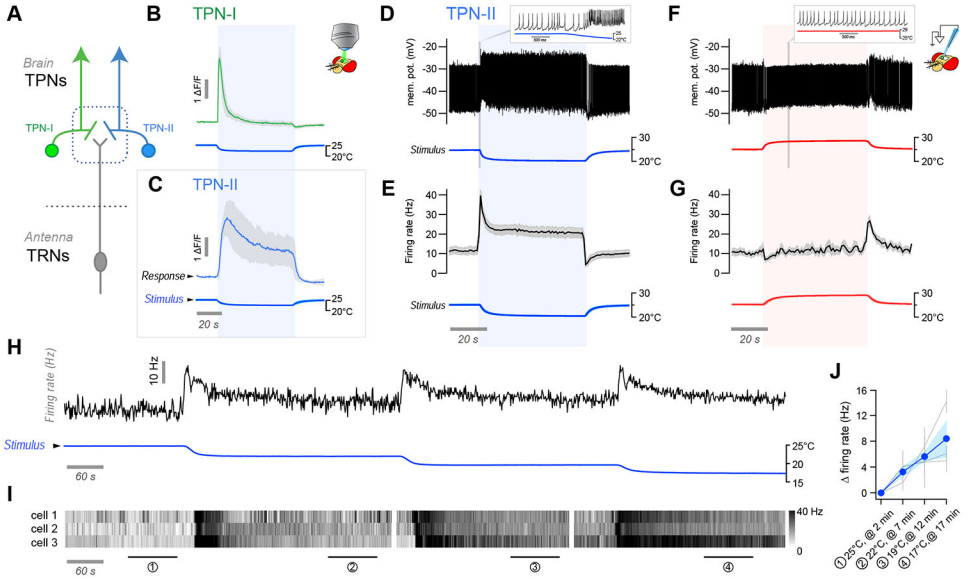

FIGURE 1 |. Identification of thermosensory projection neurons characterized by non-adapting responses

(**A**) Thermosensory projection neurons (TPNs) receive synaptic input from antennal thermoreceptors (TRNs). (**B,C**) 2-photon calcium imaging with GCaMP demonstrates significant differences in the adaptation of (**B**) type-I fast-adapting and, (**C**) type-II slow/non-adapting TPNs to a cold temperature step (~1 minute; ΔF/F traces are averages of **B**: 14 cells/3 animals, **C**: 5 cells/3 animals, ±SD; stimulus trace is an average of the experiments ± SD). (**D-G**) 2-photon guided patch clamp electrophysiology reveals that TPN-IIs' firing is indeed non-adapting. (**D**) Representative whole-cell current clamp recording from a TPN-II in response to a cold step (~5°C, 1 min.). Inset shows x-axis expansion during cooling. (**E**) Firing rate histogram for TPN-II's responses to cold (9 animals/ 9 cells, 3 trials per cell were averaged in each experiment; N=9 cells ±SEM; temp. trace: av. of 9, ±SEM). (**F,G**) TPN-IIs' are not significantly modulated by heat. (**F**) Representative whole-cell current clamp recording from a TPN-II in response to a hot step (~5°C, 1 min.). Inset shows x-axis expansion. (**G**) Firing rate histogram for TPN-II's responses to hot (5 cells/4 animals, ±SEM; temp. trace av. of 5, ±SEM). (**H-J**) TPN-IIs firing does not return to baseline even for extended cooling steps. (**H**, top) representative recording from a TPN-II subjected to extended cooling steps. (**I**) Pseudo-colored spike rate histogram of 3 cells in response to a cooling stimulus similar to that in **H** (~20 minutes recordings, 3 Δt steps as in **H**, responses aligned to stimuli). (**J**) Quantification (gray lines = mean ± SD for individual cells calculated in regions corresponding numbered bars in **I**; blue line/shading = mean ± SEM firing rate across cells, same 3 cells as in **I**).

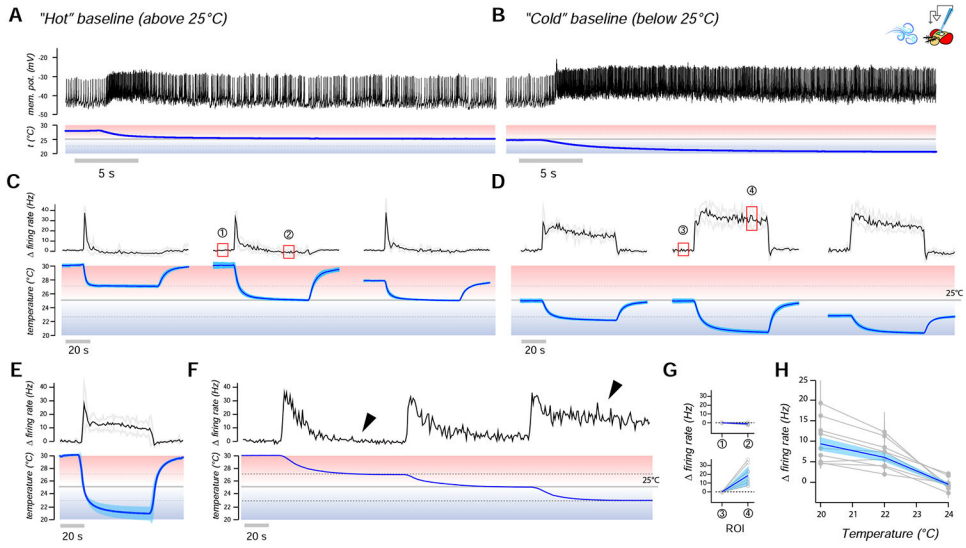

FIGURE 2 |. TPN-II neurons encode absolute temperature in the cold range

(**A-F**) Sustained firing of TPN-IIs depends on absolute temperature, rather than stimulus history. (**A,B**) Representative whole-cell current clamp recording from a TPN-II in response to a cold step starting from a baseline temperature (**A**) above or (**B**) below 25°C (see also Figure S1). (**C,D**) Firing rate histograms from TPN-II in response to cooling steps of different sizes (Δt) and settling on distinct absolute temperatures (**C**) above or (**D**) below 25°C (gray line), showing that persistent activity only appears in the cold range (below 25°C; 4 cells/4 animals, ±SD; temp. trace av. of 4, ±SD). (**E**) Sustained firing in response to a large stimulus starting at 30°C and settling to ~20°C (3 cells/3 animals, av. ±SD; temp. trace av. of 3, ±SD). (**F**) Representative response to a complex stimulus showing persistent firing below 25°C (gray line). (**G**) Quantification of firing rates corresponding to numbered ROIs in **C** and **D** (top: 10 cells/8 animals; bottom: 9 cells/9 animals). (**H**) Quantification of TPN-II firing rate changes at stable temperatures below 25°C (readings were taken after ~1 minute at each temp.; 9 cells/9 animals). In **G** and **H** responses from the same cell are connected, colored lines and shading are population averages ±SD (**G**) or ±SEM (**H**); gray dots in **H** are averages of 3 repeats/cell/condition ±SD; note that an f-test demonstrates a significant relationship between firing rates and temperature; $p<0.05$.

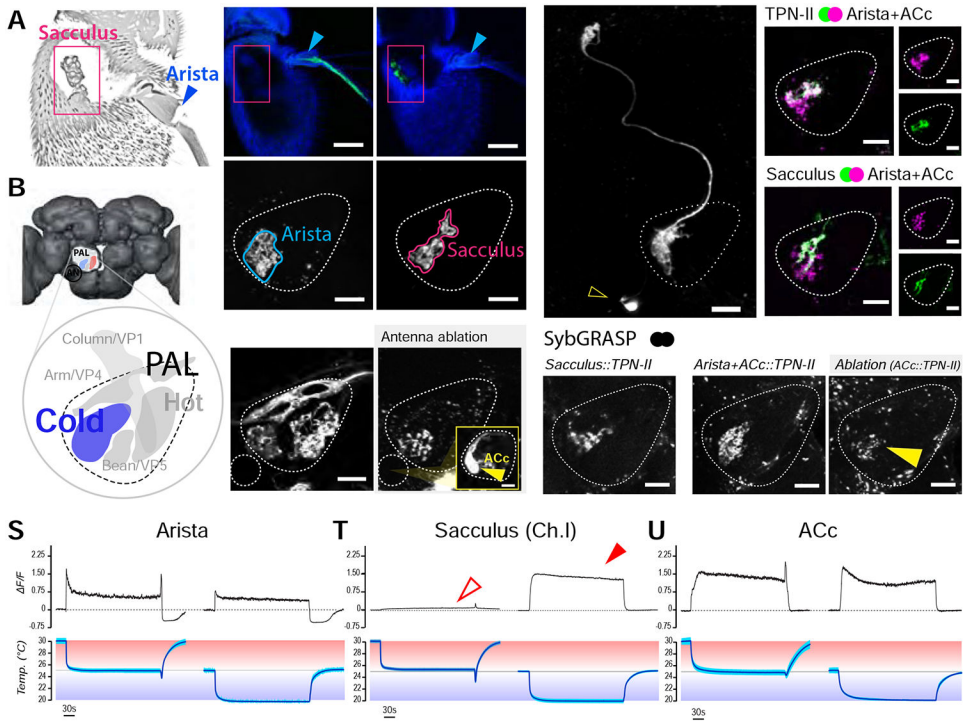

FIGURE 3 |. Three distinct populations of peripheral cold sensing neurons drive the activity of TPN-IIs

(**A**) Confocal micrograph of the fly antenna showing the location of the sacculus (pink box) and arista (blue arrow). (**B**) 3D model of the fly brain showing the location of the posterior antennal lobe (PAL) and PAL glomeruli (inset; the glomerulus innervated by cold cells is shown in blue, additional glomeruli are annotated with standard nomenclature). (**C-H**) Selective drivers identify distinct sensory neuron populations targeting the cold glomerulus. (**C,D**) A selective driver for arista cold cells labels (**C**) cell bodies in the arista and (**D**) their PAL termini. (**E,F**) A selective driver for cold cells of the sacculus labels (**E**) cell bodies innervating chamber I of the sacculus and (**F**) their termini in the PAL. (**C,E** are confocal micrographs of the whole antenna; blue: cuticle autofluorescence, green: GFP, scalebars 50μm; **D,F** are single 2-photon slices; scalebars 10μm). (**G,H**) Antenna ablation demonstrates the existence of an unusual “internal” cold receptor also innervating the PAL. (**G**) IR25a-Gal4>UAS-GFP labels many of the antennal sensory neurons innervating PAL glomeruli. (**H**) A week following antennal resection, all antennal afferents have degenerated, revealing Anterior Cold cell (ACc) termini in the PAL. The fluorescent signal can be traced to one/two cell bodies located on the edge of the antennal nerve (AN, inset –scalebar 10μm; see also Figure S2). (**I-O**) Extensive overlap between TPN-II dendrites with both arista/ACc and sacculus termini in the PAL. (**I**) A selective split-Gal4 driver reveals TPN-II’s anatomy (2-photon z-stack). (**J-O**) 2-color 2-photon micrograph illustrating spatial overlap between (**J-L**) TPN-II dendrites (green) and Arista/ACc termini (magenta, single z slice), and between (**M-O**) sacculus (green) and arista/ACc termini (magenta). (**P-R**) Synaptobrevin GRASP confirms synaptic connectivity between TPN-IIs and (**P**) sacculus, (**Q**) arista/ACc; the fact that the syb:GRASP signal in **Q** persists a week post-antenna ablation (**R**) shows ACc also connect to TPN-IIs. (**S-U**) 2-photon Ca^{2+} imaging shows sacculus neurons

exclusively respond in the cold range. Response profiles of (**S**) arista, (**T**) chamber I sacculus, and (**U**) ACc neuron termini in response to cooling steps in the hot (bottom, above 25°C, red) or cold (bottom, below 25°C, blue) range. (**S**) Arista neurons show both a transient peak in response to cooling and a persistent Ca^{2+} elevation in both conditions. (**T**) Sacculus cold cells only respond when the temperature drops below 25°C (arrows). (**U**) ACc neurons show persistent signals both above and below 25°C. **S-U** show averages of 4 animals ±SD. In all PAL panels, scale bars are 10μm.

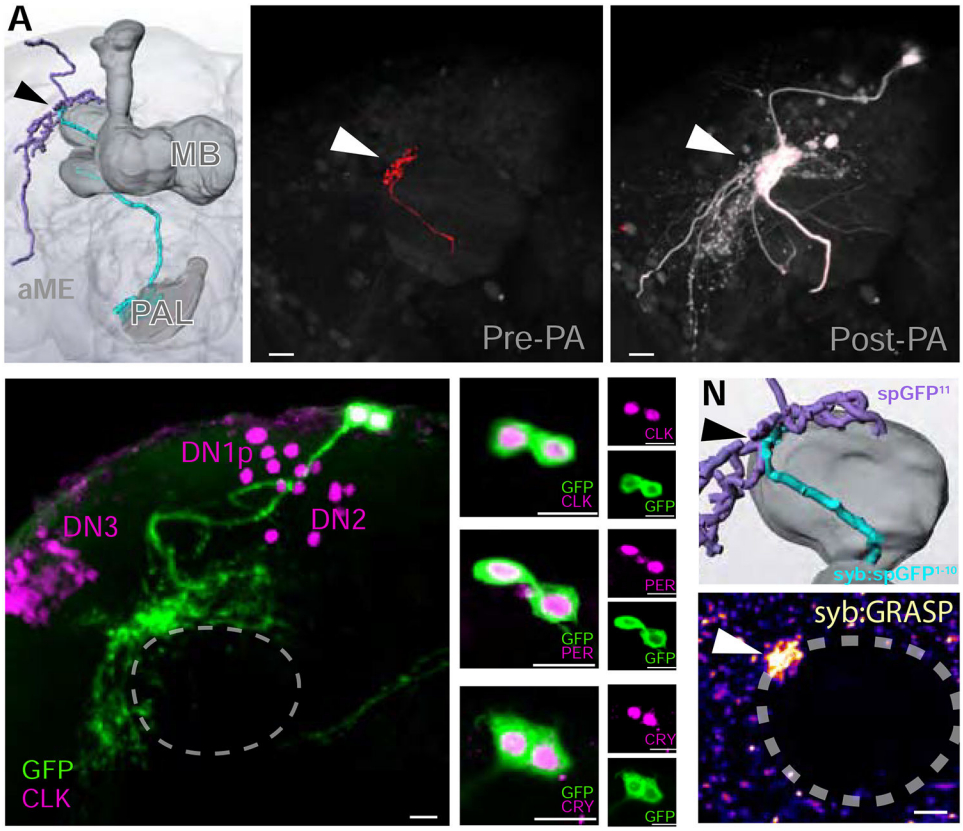

FIGURE 4 |. TPN-IIs target the DN1a group of dorsal neurons, part of the circadian clock network

(**A**) 3D reconstruction of the TPN-II (blue)-DN1a (purple) connection, at the edge of the mushroom body (MB) Calyx. (**B-C**) Photolabeling with PA-GFP reveals DN1as are candidate targets for TPN-IIs. For this experiment, (**B**, pre-photoactivation) TPN-II termini are targeted by independent labeling with TdTomato, while PA-GFP is expressed broadly. Following targeted photoactivation at 720 nm, (**C**, white) PA-GFP diffuses to label TPN-II targets. (**D-M**) DN1as are identifiable by anatomy, and because they express a combination of molecular clock components. Here, (**D**) DN1as were labeled by GFP expression (green, under the control of a selective driver) and immunostained using an anti-Clock antibody (CLK, purple; confocal z-stack of a whole-mount fly brain, note that CLK also labels DN1p, DN2, and DN3). (**E-G**) Enlargement of DN1as shown in **D**. (**H-J**) DN1as also express Period (anti-PER, purple) and (**K-M**) Cryptochrome (anti-CRY, purple; in all panels scalebar =10μm). (**N-O**) Syb:GRASP demonstrates monosynaptic connectivity between TPN-IIs and DN1as. (**N**) Enlargement of a 3D reconstruction showing predicted point of synaptic contact. (**O**) Synaptic GFP reconstitution is observed between TPN-II and DN1a neurons at the edge of the mushroom body calyx (pseudocolored 2-photon stack).

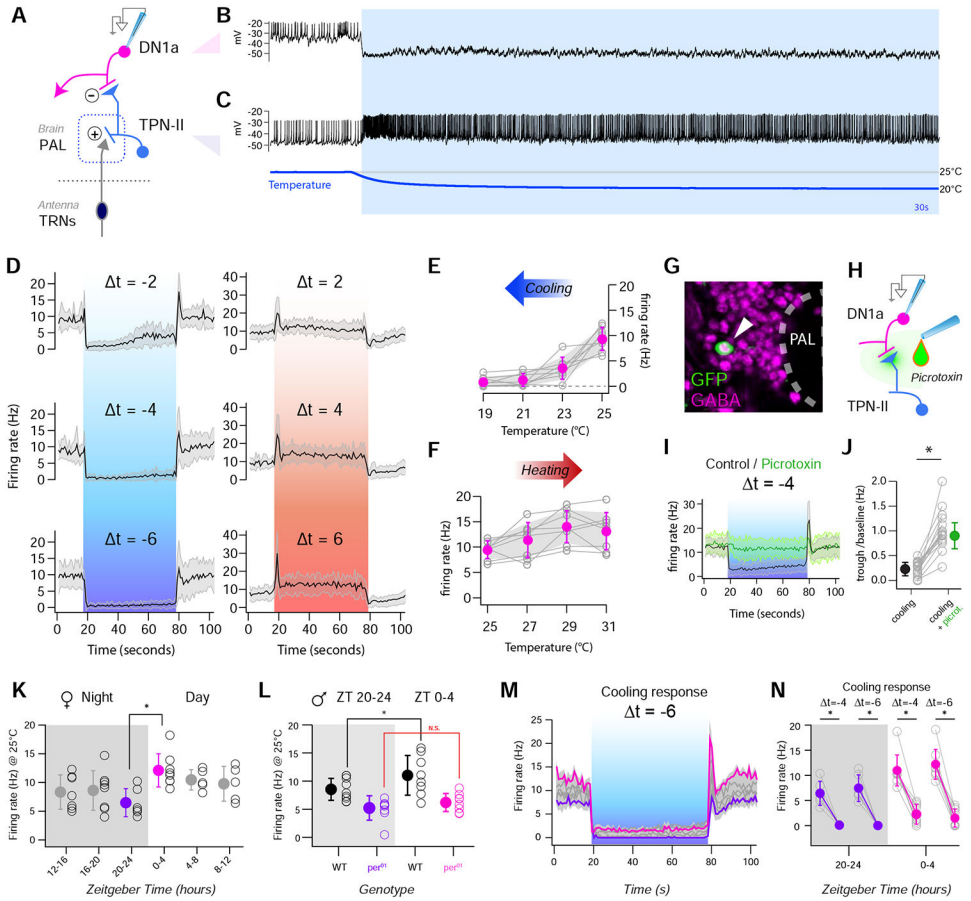

FIGURE 5 |. TPN-IIs robustly inhibit DN1a activity in cold conditions through GABA release

(**A**) Schematic representation of the circuit, including cold thermosensory neurons (TRNs, dark blue), TPN-IIs (light blue) and DN1as (pink). (**B,C**) DN1a firing is persistently silenced by cold, correlating with TPN-II activation. (**B**) Representative whole-cell current clamp recording from a DN1a neuron and (**C**) from a TPN-II in response to a cold step (recorded independently). (**D**) Average firing rate histograms for DN1as challenged with cooling steps of different amplitude show robust silencing even for small stimuli (blue boxes, Δt=−2, Δt= −4, Δt=−6; 8 cells/ 7 animals, av ±SD). Note that corresponding heating stimuli produce an initial burst in activity, but modest persistent modulation (red box, right, Δt=2, Δt=4, Δt=6; 9 cells/ 8 animals, av ±SD). (**E,F**) Quantification of firing rates at plateau for (**E**) cold and (**F**) hot steps as in **D** (gray lines connect responses from the same cell, colored dots = averages ±SD). (**G**) Whole-mount immunostaining showing that TPN-II (labeled by expression of GFP, white arrow) express the inhibitory neurotransmitter GABA (anti-GABA, pink). (**H-J**) GABA release mediates cold inhibition of DN1as. (**H**) Schematic of the experiment. (**I**) Average firing rate histograms of DN1a in response to a Δt~ −4°C cooling before (black) and after (green) application of the GABA receptor antagonist, picrotoxin (100 μM; 13 cells/13 animals, av ±SD), showing that GABA receptor blockade abolishes cold inhibition of DN1as. (**J**) Quantification of **I** as trough-to-baseline ratio of firing rate (in first 10s after cooling), before (black) and after application of picrotoxin (green). Gray circles connected by lines represent individual neurons; filled circles: population av. ± SD; * = $p < 0.05$ in a

paired, 1-tailed t-test. (**K**) Baseline firing rates of DN1as at 25°C measured during different times of day (white) and night (gray). Firing rates from different cells (black circles) were grouped in 4hr bins (filled circles, mean ± SD). Morning rates (pink) were significantly higher than evening ones (purple; N=39 cells/32 animals; * $p < 0.05$; unpaired 1-tailed t-test). (**L**) Circadian rhythms of DN1a firing are absent in per^{01} mutants. Nighttime and daytime firing rates of DN1as at 25°C recorded from WT (* $p < 0.05$, unpaired 1-tailed t-test) and period mutant flies (per^{01}, NS= not significant difference, unpaired 1-tailed t-test; black circles are individual cells, filled circles indicate av ± SD; N=35 cells/21 animals, recordings are from +/Y and per^{01}/Y male flies). (**M,N**) DN1as are inhibited by cooling at all ZTs. (**M**) Mean firing rate of DN1as in response to a cooling step (blue box, from 25°C; individual gray traces represent averages, ZTs as in **L**, ZT20–24 and ZT0–4 are colorized as in **K**; envelope: ± SEM, N=40 cells/32 animals). (**N**) Quantification of change in firing frequency in response to different cooling steps (from 25°C) during the night (ZT20–24, purple) and day (ZT0–4, pink; gray circles connected by lines indicated individual cells; filled circles indicate mean ± SD; *=$p<0.05$; paired 1-tailed t-test; 14 cells/10 animals; see also Figure S3).

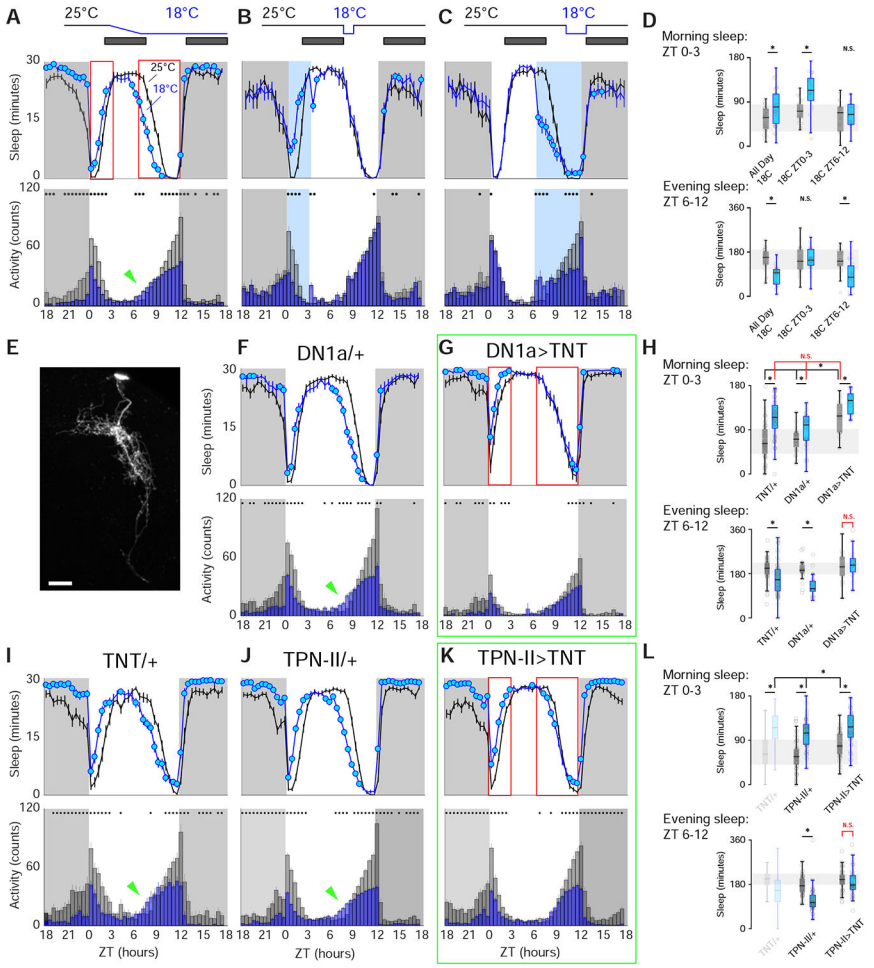

FIGURE 6 |. Genetic silencing of either DN1a or TPN-II perturbs normal daytime sleep restructuring by cold

In wild type flies, cold temperature has both acute and persistent effects on daytime activity and sleep. In (**A,F,G,I-K**) activity and sleep were quantified in 30min bins in 2 consecutive days per condition (**B,C**: 1 day/condition). Schematics on top illustrate the experimental design. Data plots represent sleep (above) and activity bar graphs (below) and are averages ±SEM across days and across individual flies; filled circles in sleep plots and black dots above activity bars indicate time points that are significantly different between cold (18°C, blue) and 25°C (gray) conditions ($p<0.05$, paired 2-sided t-test); dark shades indicate lights-off (night), ZT: zeitgeber time. (**A**) In wild-type animals, cold conditions increase morning sleep and suppresses morning activity (ZT0–3); in contrast, cold reduces both sleep and activity in the evening (ZT6–12); moreover, the onset of evening sleep is advanced (green arrowhead in **A**). As a result, the net effect of cold is an advancement of daytime sleep. (**B**) Morning cold (ZT0–3) rapidly suppresses activity and increases sleep; following the return to 25°C sleep and activity quickly return to normal levels. (**C**) Evening cold (ZT6–12) decreases sleep, so that, together, morning and evening effects recapitulate all day cold conditions (N=31 animals in **A**, 26 in **B,C**, and see **D** for quantifications). (**E**) A split-Gal4 driver allows selective targeting of DN1as (shown driving GFP; 2-photon z-stack, scale bar =20μm). (**F-L**) Silencing DN1as or TPN-IIs using selective split-Gal4s perturbs sleep

restructuring by cold temperature. (**F,I,J**) Control genotypes. (N=30 in **F**, N=61 in **I**, N=62 in **J**). (**G**) Silencing DN1as by expression of tetanus toxin light chain (TNT) partially mimics cold conditions, producing flies that sleep more in the morning even at 25°C, and that fail to restructure their afternoon sleep in response to cold; (N=19 animals). (**K**) Silencing TPN-II output with TNT also produces flies that fail to restructure afternoon sleep in response to cold (N=52 animals; see **H, L** for quantifications; In all boxplots, box edges: 25th and 75th percentiles; thick lines: median; whiskers: data range; gray dots: individual data points/flies; *=$p<0.05$ in paired 2-sided t-test comparing 25°C vs 18°C within genotype or 2-way ANOVAs with a Bonferroni correction for multiple comparisons across genotypes/temperatures; NS= no significant difference).

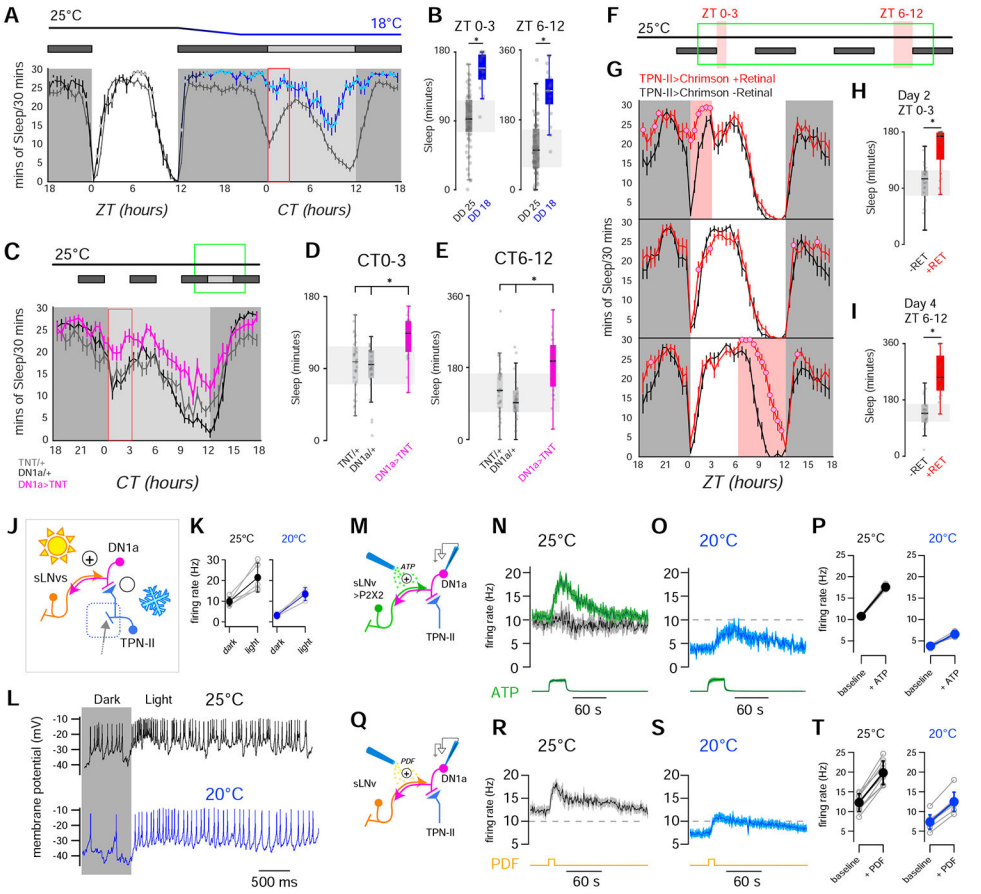

FIGURE 7 |. Sleep and DN1a activity are modulated by the opposing pushes of light and cold temperature

(**A,B**) Cold and dark synergize to increase sleep across the day. (**A**, top) Behavioral protocol used to evaluate sleep on flies entrained in 12hrs Light-Dark (LD) cycles (white box: day (lights on), black box: night (lights off); gray box: subjective day (lights off)). (**A**, bottom) Sleep plot for two independent groups of control (wild type) flies during a single LD day at 25°C and in the following dark day at either 18°C (blue line N=19 animals, ± SEM) or 25°C (gray line; N=19 animals, ± SEM; filled circles indicate time points that are significantly different between conditions; $p<0.05$, unpaired 2-sided t-test). (**B**) Quantification of total sleep in the indicated intervals (box edges: 25th and 75th percentiles; thick lines: median; whiskers: data range; gray dots: individual datapoints/flies; *=$p<0.05$ in unpaired 2-sided t-test). (**C-E**) In the dark, suppressing DN1a output by TNT expression mimics cold conditions, increasing sleep across the day. (**C**, top) Behavioral protocol. (**C**, bottom) Sleep in DN1a>TNT flies (orange trace; N=25 animals), UAS-TNT/+ (gray; N=32 animals) and DN1a-Gal4/+ flies (black; N=31 animals, all traces are: AV± SEM, circles= significantly different from both controls in 2-way ANOVA, $p<0.05$). (**D,E**) Quantification of total sleep in the indicated intervals for genotypes in **C** (box edges: 25th and 75th percentiles; thick lines: median; whiskers: data range; gray dots: individual data points/flies; *= $p<0.05$, 2-way ANOVA with a Bonferroni correction for multiple comparisons across genotypes). (**F-I**) Optogenetic activation of TPN-II produces an acute increase in sleep. (**F**) Protocol used (3 consecutive days represented top to bottom), red shading indicates optogenetic activation.

(**G**) Sleep pattern of TPN-II>Chrimson flies fed all-trans retinal (red trace; 25 animals) or control food (black; 27 animals -note that retinal is essential for Chrimson function; traces: AV± SEM, circles= significantly different from controls in 2-sided t-tests, p<0.05). (**H, I**) Quantification of total sleep in the indicated intervals (**H**) ZT0–3 on day 2, and (**I**) ZT6–12 on day 4 (box edges: 25th and 75th percentiles; thick lines: median; whiskers: data range; gray dots: individual data points (flies); *=p<0.05, unpaired, 2-sided t-test). (**J**) Circuit schematic including TPN-IIs (light blue), DN1as (pink) and sLNvs (orange). (**K,L**) DN1as are excited by light. (**K**) Light produces robust increases in firing rate at 25°C (black) and at 20°C (blue; gray circles connected by lines represent individual cells; filled circles are av ± SD, * p < 0.05, paired 1-tailed t-test). (**L**) Representative whole-cell recordings from a single DN1a neuron before and during light stimulation (yellow box), at 25°C (black) or 20°C (blue). (**M**-**P**) Artificial activation of sLNvs drives fire rate increases in DN1a and can overcome cold inhibition. (**M**) Experiment schematic. sLNvs express the exogenous ATP receptor P2X2 and can be activated by pressure ejection of ATP (20mM, green), while patch-clamp records activity in DN1a (pink). (**N**) ATP (20 mM, green) can drive an increase in DN1a firing at 25°C in animals in which sLNvs express P2X2 (green trace, 4 cells/ animals), but not in control animals (driver without the receptor, gray/black trace; 6 cells/ 4 animals). (**O**) ATP can also overcome cold inhibition of DN1as (4 cells/4 animals av ± SEM; the green trace at the bottom of **N** and **O** is Alexa594 fluorescence, a dye included as a marker in the ATP solution, arbitrary fluorescence units ± SEM). (**P**) Quantification of **N** and **O** (gray circles connected by lines represent individual cells; filled circles are av ± SD, * p < 0.05, paired 1-tailed t-test). (**Q**-**T**) The neuropeptide PDF can increase DN1a firing to overcome inhibition in the cold. (**Q**) Experiment schematic. PDF is pressure ejected (50μM, yellow), while patch-clamp records activity in DN1a (pink). (**R**-**T**) PDF can drive an increase in DN1a firing both at (**R**) 25°C or (**S**) 20°C (9 cells/6 animals av ± SD; the yellow line at the bottom of **R** and **S** represent the approximate time of the PDF puff). (**T**) Quantification of **R** and **S** (gray circles connected by lines represent individual cells; filled circles are av ± SD, * p < 0.05, paired 1-tailed t-test; all experiments were done at ZT 0–8).

REAGENT or RESOURCE	SOURCE	IDENTIFIER
Antibodies		
chicken polyclonal anti-GFP	Abcam	Cat# ab13970, RRID:AB_300798
donkey polyclonal anti-mouse Alexa 594	Abcam	Cat# ab150105, RRID:AB_2732856
chicken polyclonal anti-GFP	Abcam	Cat# ab13970, RRID:AB_300798
rat monoclonal anti-Elav	Developmental Studies Hybridoma Bank	Cat# Rat-Elav-7E8A10 anti-elav, RRID:AB_528218
mouse monoclonal anti-Repo	Developmental Studies Hybridoma Bank	Cat# 8D12 anti-Repo, RRID:AB_528448
rabbit anti-Per	Gift from R. Allada & M. Rosbash	
rabbit anti-Cry	Gift from R. Allada	
donkey polyclonal anti-chicken Alexa 488	Jackson ImmunoResearch Labs	Cat# 703-545-155, RRID:AB_2340375
donkey polyclonal anti-rabbit Alexa 594	Jackson ImmunoResearch Labs	Cat# 711-585-152, RRID:AB_2340621
donkey polyclonal anti-chicken Alexa 488	Jackson ImmunoResearch Labs	Cat# 703-545-155, RRID:AB_2340375
rabbit polyclonal anti-GABA	Millipore Sigma	Cat# A2052, RRID:AB_477652
goat anti-rat DyLight 594	NovusBio	Cat# NBP1–76096, RRID:AB_11023227
goat polyclonal anti-CLK (dC-17)	Santa Cruz Biotechnology	Cat# sc-27070, RRID:AB_638555
rabbit polyclonal anti-dsRED	Takara Bio	Cat# 632496, RRID:AB_10013483
donkey polyclonal anti-goat Alexa 568	Thermo Fisher Scientific	Cat# A-11057, RRID:AB_2534104
Chemicals, Peptides, and Recombinant Proteins		
Adenosine 5′-triphosphate magnesium salt	Millipore Sigma	Cat. # A9187; CAS: 74804-12-9
Pigment dispersing factor (PDF) peptide	Gift from R. Allada; Genscript	
Alexa Fluor 594 Hydrazide	Thermo Fisher Scientific	Cat. # A10438
all trans-Retinal	Millipore Sigma	Cat. # R2500; CAS: 116-31-4
picrotoxin	Tocris	Cat. # 1128; CAS: 124-87-8
Experimental Models: Organisms/Strains		
D. melanogaster: IR25a Gal4	Bloomington Drosophila Stock Center	BDSC: 41728; Flybase: FBti0148895
D. melanogaster: R49B06 Gal4	Bloomington Drosophila Stock Center	BDSC: 50409; Flybase: FBti0136309
D. melanogaster: R49B06 LexA	Bloomington Drosophila Stock Center	BDSC: 52707; Flybase: FBti0155964
D. melanogaster: R25B07 AD	Bloomington Drosophila Stock Center	BDSC: 70144; Flybase: FBti0188065
D. melanogaster: R25B07 LexA	Bloomington Drosophila Stock Center	BDSC: 54125; Flybase: FBti0155514
D. melanogaster: R77C10 Gal4	Bloomington Drosophila Stock Center	BDSC: 39958; Flybase: FBti0138389
D. melanogaster: R77C10 DBD	Bloomington Drosophila Stock Center	BDSC: 69705; Flybase: FBti0191888
D. melanogaster: R60H12 AD	Bloomington Drosophila Stock Center	BDSC: 70761; Flybase: FBti0188587
D. melanogaster: VT032805 DBD	Bloomington Drosophila Stock Center	BDSC: 75119; Flybase: FBti0193574
D. melanogaster: R49A06 Gal4	Bloomington Drosophila Stock Center	BDSC: 50401; Flybase: FBti0136298
D. melanogaster: R23E05 Gal4	Bloomington Drosophila Stock Center	BDSC: 49029; Flybase: FBti0134061
D. melanogaster: R23E05 AD	Bloomington Drosophila Stock Center	BDSC: 70601; Flybase: FBti0188021
D. melanogaster: R92H07 DBD	Bloomington Drosophila Stock Center	BDSC: 70004; Flybase: FBti0192102
D. melanogaster: 20XUAS-IVS-GCaMP6f	Bloomington Drosophila Stock Center	BDSC: 42747; Flybase: FBti0151345

REAGENT or RESOURCE	SOURCE	IDENTIFIER
D. melanogaster: 20XUAS-IVS-jGCaMP7f	Bloomington Drosophila Stock Center	BDSC: 79031; Flybase: FBti0199863
D. melanogaster: 20XUAS-IVS-CsChrimson.mVenus	Bloomington Drosophila Stock Center	BDSC: 55135; Flybase: FBti0160803
D. melanogaster: 13XLexAop-IVS-jGCaMP7f	Bloomington Drosophila Stock Center	BDSC: 80914; Flybase: FBti0202387
D. melanogaster: AOP.Syb:spGFP[1–10],UAS.spGFP[11]	Bloomington Drosophila Stock Center	BDSC: 64315; Flybase: FBti0180566; FBti0180561
D. melanogaster: 10XUAS-IVS-mCD8::GFP	Bloomington Drosophila Stock Center	BDSC: 32186; Flybase: FBst0032186
D. melanogaster: UAS-TNT	kind gift from M. Rosbash	
D. melanogaster: LexAop-P2X2	kind gift of O. Shafer	
D. melanogaster: 13XLexAop-TdTomato	kind gifts from V. Ruta and B. Noro	
D. melanogaster: UAS-C3PA	kind gifts from V. Ruta and B. Noro	
D. melanogaster: UAS-SPA	kind gifts from V. Ruta and B. Noro	
D. melanogaster: Synaptobrevin-Gal4	kind gifts from V. Ruta and B. Noro	
D. melanogaster: $w^{1118\ CS}$	kind gifts of R. Allada	
D. melanogaster: per^{01}	kind gifts of R. Allada	
D. melanogaster: VT003226 Gal4	Vienna Drosophila Resource Center	
Software and Algorithms		
MATLAB	The Mathworks	http://www.mathworks.com
Fiji	Schneider et al., 2012	http://fiji.sc
Pclamp (Clampex software v.9.2.1.9)	Axon Instruments/Molecular Devices	https://www.moleculardevices.com/
Igor Pro v.6.37	Wavemetrics, Inc.	https://www.wavemetrics.com/
Neuromatic v2.6i plug-in for Igor Pro	Rothman and Silver, 2018	http://www.neuromatic.thinkrandom.com/
Axograph v.1.70	Axograph	https://axograph.com/